

Quantum chaos in the presence of nonconformality

Ashis Saha^{*} and Sunandan Gangopadhyay[†]

*Department of Astrophysics and High Energy Physics, S.N. Bose National Centre for Basic Sciences,
JD Block, Sector-III, Salt Lake, Kolkata 700106, India*



(Received 21 February 2024; accepted 2 July 2024; published 26 July 2024)

The behavior of a chaotic system and its effect on existing quantum correlation has been holographically studied in the presence of nonconformality. Keeping in mind the gauge/gravity duality framework, the nonconformality in the dual field theory has been introduced by considering a Liouville type dilaton potential for the gravitational theory. The resulting black brane solution is associated with a parameter η which represents the deviation from conformality. The parameters of chaos, namely, the Lyapunov exponent and butterfly velocity are computed by following the well-known shock wave analysis. The obtained results reveal that the presence of nonconformality leads to suppression of the chaotic nature of a system. Further, for a particular value of the nonconformal parameter η , the system achieves Lyapunov stability resulting from the vanishing of both the Lyapunov exponent as well as butterfly velocity. Interestingly, this particular value of η matches with the previously given upper bound of η known as Gubser bound in the literature. The effects of chaos and nonconformality on the existing correlation of a thermofield doublet state have been quantified by holographically computing the thermomutual information in both the presence and absence of the shock wave. Furthermore, the entanglement velocity is also computed, and the effect of nonconformality on it has been observed. Finally, the obtained results for the Lyapunov exponent and the butterfly velocity have also been computed from the pole-skipping analysis. The results from the two approaches agree with each other.

DOI: [10.1103/PhysRevD.110.026025](https://doi.org/10.1103/PhysRevD.110.026025)

I. INTRODUCTION

The study of various properties of a chaotic system has always been a matter of great interest both theoretically and experimentally. For a classical system, the characterization of chaos is done with help of a parameter known as the Lyapunov exponent λ_L which can be defined in the following way:

$$\lambda_L \sim \frac{1}{t} \ln \left(\frac{\delta \xi(t)}{\delta \xi_0} \right), \quad (1)$$

where $\delta \xi(t)$ denotes the change in the phase-space trajectory of a classical dynamical system due to a change in the initial condition $\delta \xi_0$. The above relation also advocates for the fact that chaos is highly sensitive to the initial conditions. On the other hand, the study of chaos in case of

a quantum many body system is quite nontrivial [1]. Traditionally, one characterizes chaos for a nonclassical system by comparing its energy spectrum to the spectrum of random matrices [2]. Apart from this approach, another way to probe quantum chaos is to compute the *double commutator* of two generic local Hermitian operators $\hat{V}(0)$ and $\hat{W}(x, t)$. This can be written down in the following way [3]:

$$\begin{aligned} \mathcal{C}(x, t) &= -\langle [\hat{W}(x, t), \hat{V}(0)]^2 \rangle_\beta \\ &= -\langle \hat{W}(x, t) \hat{V}(0) \hat{W}(x, t) \hat{V}(0) \rangle_\beta. \end{aligned} \quad (2)$$

The above quantity $\mathcal{C}(x, t)$ measures how much effect the perturbation $\hat{V}(0)$ at an earlier time creates on the later measurement of $\hat{W}(x, t)$. In other words, one intends to study at what rate the information gets transferred between two spacelike separated points. This property leads to the phenomenon *velocity of the butterfly effect* or commonly known as the *butterfly velocity* [4,5]. The butterfly velocity is a state dependent quantity and can be understood as the low energy analog of the *Lieb-Robinson velocity* [6]. This implies that it acts as a bound for the rate of transfer of information for a quantum mechanical system at low energy scale. For large- N gauge theories, the four-point

^{*}Contact author: ashis.saha@bose.res.in

[†]Contact author: sunandan.gangopadhyay@bose.res.in

Published by the American Physical Society under the terms of the Creative Commons Attribution 4.0 International license. Further distribution of this work must maintain attribution to the author(s) and the published article's title, journal citation, and DOI. Funded by SCOAP³.

correlator has the following form which stands to be very crucial for the study of quantum chaos [4,7,8]:

$$\mathcal{C}(x, t) \sim \exp \left[\lambda_L \left(t - t_* - \frac{|x|}{v_B} \right) \right], \quad (3)$$

where λ_L is the Lyapunov exponent, and v_B is the butterfly velocity. It is worth noting that in the above relation, λ_L is sometimes said to be the quantum mechanical analog of the classical Lyapunov exponent [9] which characterizes the growth of quantum chaos. The Lyapunov exponent satisfies the well-known MSS (Maldacena-Shenker-Stanford) bound $\lambda_L \leq \frac{2\pi}{\beta}$, where, β is the inverse of Hawking temperature [10]. The bound is only saturated for maximally chaotic systems. Furthermore, the relation [given in Eq. (3)] is true as long as $t_{dis} \ll t < t_*$, where, t_{dis} is the *dissipation time* which controls the late time behavior of $\mathcal{C}(x, t)$ and t_* is the *scrambling time* at which $\mathcal{C}(x, t)$ becomes $\sim \mathcal{O}(1)$ [11]. The scrambling time basically denotes the timescale at which the given perturbation gets distributed among all the degrees of freedom of the chaotic quantum mechanical system. From Eq. (3), one can observe that the spacelike separation between the operators further delays the scrambling of information in the system. On the other hand, the butterfly velocity characterizes the growth of the given perturbation $\hat{V}(0)$. This motivates one to define a *butterfly effect light cone* $t - t_* = \frac{|x|}{v_B}$ for the double commutator given in Eq. (2). Inside the cone ($t - t_* > \frac{|x|}{v_B}$), $\mathcal{C}(x, t) \sim \mathcal{O}(1)$, and outside the cone ($t - t_* < \frac{|x|}{v_B}$), $\mathcal{C}(x, t) \approx 0$.

The initial motivation to study chaos in a holographic setup lies in the understanding that black holes are intrinsically thermal systems which are characterized by the Hawking temperature, and it is a well-known fact that thermal systems are the primary playgrounds for chaos. Further, it has been noted that for black holes, the MSS bound is always saturated [4,10] which depicts the fact that the black holes are always maximally chaotic, or in other words, they are the fastest scramblers [12,13]. Keeping this observation in mind along with the gauge/gravity duality [14–16], one might propose the following. The holographic description¹ of a maximally chaotic finite temperature large- N gauge theory is possible as long as the Lyapunov exponent saturates the MSS bound. Another interesting fact that we would like to mention is the following. Inclusion of higher-curvature corrections on the gravity side does not modify the MSS bound; that is, the bound still remains $\lambda_L = \frac{2\pi}{\beta}$ [8]. However, the presence of higher-curvature corrections do change the

¹Existence of a one spatial dimension higher gravity solution is said to be the holographic description of a control field theory in one spatial dimension less.

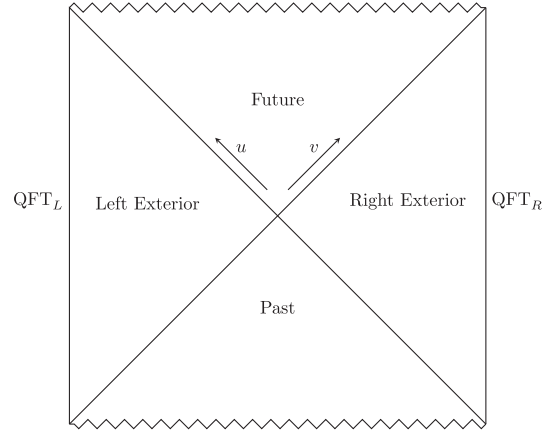


FIG. 1. Dual geometry of the thermofield doublet state.

butterfly velocity [8,17,18]. The conventional approach to holographically study quantum chaos relies on the dual description of the thermofield doublet (TFD) state [19,20]. This consists of two completely disjoint quantum mechanical systems Quantum Field Theory (QFT) QFT_L and QFT_R along with their energy eigenstates denoted as $|n\rangle_L$ and $|n\rangle_R$. In this setup, the TFD state can be defined as

$$|\text{TFD}\rangle = \frac{1}{\sqrt{Z}} \sum_n e^{-\frac{\beta E_n}{2}} |n\rangle_L \otimes |n\rangle_R. \quad (4)$$

The holographic description of the TFD state is a two-sided eternal black hole geometry in anti-de Sitter (AdS) spacetime where the two black hole geometries are connected with each other by a nontraversable wormhole. The quantum theories are living on the two asymptotic boundaries (left and right) of the black hole spacetimes (a simple visualization of this setup has been given in Fig. 1). As we mentioned earlier, the associated geometries of the asymptotic boundaries are connected with each other via a nontraversable wormhole, and this ensures that the quantum theories (living on these boundaries) do not interact with each other. Entanglement is the sole reason due to which they are aware of each other. The TFD state implies that if we consider subsystems, namely, A and B which belong to the systems QFT_L and QFT_R respectively then there exists a nonvanishing local correlation between A and B . One can quantify this correlation with the help of the holographic thermomutual information (HTMI) $I(A:B)$ which has the following definition [21]:

$$I(A:B) = S_{\text{vn}}(A) + S_{\text{vn}}(B) - S_{\text{vn}}(A \cup B), \quad (5)$$

where $S_{\text{vn}}(\cdot)$ denotes the von Neumann entropy corresponding to the relevant subsystem. The holographic thermomutual information is the generalization of the holographic mutual information [22–24] which was first introduced in [21]. The computation of HTMI requires a wormhole which connects the asymptotic boundaries of a

two-sided eternal black hole geometry in AdS. Similar to HTMI, the HTMI is also UV finite and positive definite quantity. In the absence of chaos, HTMI is nonzero and positive which depicts the signature of entanglement between the subsystems A and B [21,22,24]. In order to observe the butterfly effect one needs to disrupt the existing local correlation between the subsystems of two copies of decoupled quantum systems. In other words, one has to disrupt the structure of TFD given in Eq. (4). In a holographic setup, this can be done by adding a small perturbation to the system in the asymptotic past. From the bulk perspective, the energy of the small perturbation (which has been added to the system at an early enough time) gets blueshifted and falls to the black hole which results in the shock wave modification of the existing holographic geometry [25,26]. The mentioned process of perturbing the TFD structure disrupts the previously existing local correlation between the subsystems, and then one can follow the approach shown in [4,27] in order to obtain the Lyapunov exponent and butterfly velocity. Some of the recent works in this direction can be found in [28–35]. It is to be noted that the mentioned perturbation disrupts the correlation between the two decoupled theories living at the two boundaries of the two-sided eternal black hole geometry. In other words, it will only affect the term $S_{\text{vn}}(A \cup B)$, not the individual entanglement pattern $S_{\text{vn}}(A)$ or $S_{\text{vn}}(B)$. Furthermore, the disruption of this two-sided correlation is controlled by the *entanglement velocity* v_{en} which basically probes the linear growth of $S_{\text{vn}}(A \cup B)$ for ($t_e \geq t_*$) in the following way [36–38]:

$$\frac{dS_{\text{vn}}(A \cup B)}{dt_e} = v_{\text{en}} S_{\text{th}} \text{Area}_{\Sigma}, \quad (6)$$

where t_e denotes the time at which the perturbation is added to the system and $\text{Area}_{\Sigma} = \partial(A \cup B)$. Further, S_{th} is the density of the thermal entropy (Bekenstein-Hawking entropy of the black hole). This behavior has been noted in both purely field theoretic setup [39,40] and holographic setup, and it can be explained with the help of the *entanglement tsunami* phenomena [41,42]. In [38], it has been argued that the entanglement velocity is always bounded from above by the butterfly velocity for any holographic theory obeying the null energy condition, that is,

$$v_{\text{en}} \leq v_B. \quad (7)$$

Further, in [43], it was proven that the above relation holds for any unitary quantum system. It is to be noted that both the butterfly velocity and entanglement velocity are always less than the speed of light [43,44] due to causality. On other hand, recently, it was shown that in case of a quantum many body system, properties of a chaotic system can be characterized with the help of the energy density retarded Green's function [17,45,46]. In the context of AdS/CFT duality,

the mentioned Green's function can be written down in the following form [47,48]:

$$G_{T^{00}T^{00}}^R = \frac{b(\omega, k)}{a(\omega, k)}. \quad (8)$$

Now, the ‘‘pole-skipping’’ phenomena [49,50] states that at some special points of the complex (ω, k) plane, $b(\omega_*, k_*) = a(\omega_*, k_*) = 0$ where (ω_*, k_*) denotes the mentioned special point. This implies that, at these special points, one has a line of zeroes intersecting with the line of poles for the retarded Green's function. Further, this implies that at these points the retarded Green's function is nonunique or ill defined. We follow the literature and denote these points as the pole-skipping points. For theories with holographic duals, the pole-skipping points can be obtained from the bulk field equations [45,46,51,52]. In the holographic setup, the nonuniqueness of the retarded Green's function corresponding to the boundary theory is mapped to the nonuniqueness of the ingoing mode of the bulk field at the event horizon. It has been observed that for a static black hole, the pole-skipping frequency (leading order) is given by [53–56]

$$\omega_* = 2\pi i T(s - 1), \quad (9)$$

where s represents the spin of the field operator. The above relation implies that depending upon the spin of the field, the position of the pole-skipping frequency varies in the complex- ω plane. Further, it has been observed that for strongly coupled theories with holographic duals, the leading order pole-skipping point located in the upper half of the complex- ω plane is related to the Lyapunov exponent and the Butterfly velocity in the following way [17,45,57]:

$$\omega_* = i\lambda_L; \quad k_* = \frac{i\lambda_L}{v_B} \equiv \frac{\omega_*}{v_B}. \quad (10)$$

However, the above observation is only true for strongly coupled theories with holographic dual which are maximally chaotic. For nonmaximally chaotic (strongly coupled) systems this is not true as only for the maximally chaotic systems, the stress tensor dominates chaos, and pole skipping only recovers the contributions of the stress tensor to the Lyapunov exponent and butterfly velocity [58]. From the subsequent discussion, we shall find that the results in this paper are compatible with the conclusions drawn in [58]. The above relation of the Lyapunov exponent together with the relation given in Eq. (9) depicts the fact that only for $s = 2$ field (metric fluctuation) one gets the pole-skipping points in the upper half of the complex- ω plane, which are related to the parameters of chaos. Furthermore, one can also observe that for $s = 2$, one gets a maximally chaotic system as in this case, $\lambda_L = 2\pi T$ (saturated MSS bound). On the other hand, for other fields ($s = 0, \frac{1}{2}, 1$, etc.), the pole-skipping point is not related to the parameters of chaos

although the retarded Green's function is still nonunique at the pole-skipping points [54]. Some interesting works in this direction can be found in [18,53–55,58–77].

In this work we consider the black brane solution of the Einstein-dilaton theory with a Liouville type profile for the dilaton potential [78–81] as the gravitational theory. The motivation to consider such a theory lies in the fact that in the asymptotic limit we get a warped geometry instead of an AdS geometry. This in turn means that in the context of gauge/gravity duality, the boundary field theory will be relativistic but nonconformal in nature [82]. This type of geometry belongs to the class of geometries (such as Lifshitz geometry, hyperscaling violating geometry, anisotropic geometry, etc.) which help us to generalize the gauge/gravity duality. The geometry under consideration is characterized by the parameter η . In the limit $\eta \rightarrow 0$, we obtain the Schwarzschild type black brane solution. This nonconformal parameter also satisfies a certain bound known as the Gubser bound [83,84].

The plan of this paper is as follows. In Sec. II, we briefly discuss the holographic gravitational dual of the nonconformal theory. We then compute the corresponding shock wave geometry and compute the Lyapunov exponent and butterfly velocity in Sec. III. In Sec. IV, we quantify the effect of shock wave on the holographic thermomutual information and also compute the entanglement velocity. We once again compute the Lyapunov exponent and butterfly velocity from the lowest order pole-skipping points. This we provide in Sec. V. In this section, we also compute the higher order pole-skipping points by considering scalar field fluctuations. We summarize our findings in Sec. VI.

II. EINSTEIN-DILATON THEORY WITH LIOUVILLE POTENTIAL

The Einstein-Hilbert action corresponding to the $(d+1)$ -dimensional Einstein-dilaton theory with Liouville type potential reads as [78–81]

$$S_{\text{EH}} = \frac{1}{16\pi G_N^{d+1}} \int d^{d+1}x \sqrt{-g} [R - 2(\partial\phi)^2 - V(\phi)], \quad (11)$$

where $V(\phi) = 2\Lambda e^{\eta\phi}$ is the Liouville type dilaton potential. Here Λ represents the cosmological constant $\Lambda < 0$, and η denotes the nonconformal parameter which captures the deviation of the system from conformality. Further, $\eta < \sqrt{\frac{8d}{(d-1)}}$ [83,84]. The corresponding Einstein field equations and the equation of motion for the dilaton field reads as

$$R_{\mu\nu} - \frac{1}{2}g_{\mu\nu}R + \frac{1}{2}g_{\mu\nu}V(\phi) = 2\partial_\mu\phi\partial_\nu\phi - g_{\mu\nu}(\partial\phi)^2$$

$$\frac{1}{\sqrt{-g}}\partial_\mu(\sqrt{-g}g^{\mu\nu}\partial_\nu\phi) = \frac{1}{4}\frac{\partial V(\phi)}{\partial\phi}. \quad (12)$$

By solving the above two equations, one can obtain the following nonconformal black brane geometry² [78–81,85]:

$$ds^2 = -r^{2p}f(r)dt^2 + \frac{dr^2}{r^{2p}f(r)} + r^{2p}\sum_{i=1}^{d-1}dx_i^2$$

$$f(r) = 1 - \left(\frac{r_+}{r}\right)^c, \quad (13)$$

where we have used

$$p = \frac{8}{8 + (d-1)\eta^2}; \quad c = \frac{8d - (d-1)\eta^2}{8 + (d-1)\eta^2}. \quad (14)$$

As mentioned earlier, the asymptotic limit of the above given black brane is not AdS, and therefore the boundary field theory is not conformal. Further, it can be observed that in the limit $\eta \rightarrow 0$, one obtains the AdS _{$d+1$} -Schwarzschild black brane solution. Recently, in [86,87], the authors have applied two different types of scalar potentials to numerically construct the solutions of hairy black holes and scalarons to study their properties systematically. These hairy black holes also bifurcated from the Schwarzschild black hole.

The Hawking temperature of the black brane geometry [given in Eq. (13)] reads as

$$T_H = \frac{k}{2\pi} = \left(\frac{c}{4\pi}\right)r_+^{2p-1}, \quad (15)$$

where k is the surface gravity. It is to be observed that for $\eta = \sqrt{\frac{8d}{(d-1)}}$, the Hawking temperature of the black brane is zero, irrespective of the value of r_+ . Furthermore, from the above relation, one can express the event horizon position r_+ in terms of the Hawking temperature. This reads as

$$r_+ = \left(\frac{c}{4\pi T_H}\right)^{\frac{1}{1-2p}} = \left(\frac{\beta c}{4\pi}\right)^{\frac{1}{1-2p}}. \quad (16)$$

III. SHOCK WAVE ANALYSIS: LYAPUNOV EXPONENT AND BUTTERFLY VELOCITY

In this section, we now proceed to compute the Lyapunov exponent and butterfly velocity by carrying out the shock wave analysis. In order to obtain the shock wave geometry in this setup, we first write down the metric [given in Eq. (13)] in the Kruskal coordinates as it provides convenience in case of a two-sided geometry setup.

²We have set $G_N = 1$ and AdS radius $R = 1$, for the sake of simplicity.

The first step is to introduce the Tortoise coordinate. For a general metric of the form

$$ds^2 = -G_{tt}(r)dt^2 + G_{rr}(r)dr^2 + G_{ij}(r)dx^i dx^j, \quad (17)$$

the Tortoise coordinate is defined as

$$dr_* = -\sqrt{\frac{G_{rr}(r)}{G_{tt}(r)}} dr. \quad (18)$$

For the metric given in Eq. (13), the above equation leads to

$$dr_* = -\frac{dr}{r^{2p} f(r)}. \quad (19)$$

With the above transformation in hand, we now move on to the following Kruskal coordinates:

$$u = e^{-k(t-r_*)}, \quad v = -e^{k(t+r_*)}. \quad (20)$$

By incorporating the Kruskal coordinate transformation, one obtains the following form:

$$ds^2 = 2\Omega(u, v)dudv + g_{ij}(u, v)dx^i dx^j, \quad (21)$$

where

$$2\Omega(u, v) = \frac{\beta^2 r^{2p} f(r)}{4\pi^2 uv}. \quad (22)$$

In Kruskal coordinates, the event horizon lies at $u = 0$ or $v = 0$. The exterior regions are located at $u > 0, v < 0$ (right exterior) or $u < 0, v > 0$ (left exterior). On the other hand, the singularity is located at $uv = 1$, and the boundary is at $uv = -1$. In Fig. 1, we have given the Penrose-Carter diagram depicting all the facts mentioned above. One can now assume the following general form of the stress tensor [26] corresponding to the unperturbed metric given in Eq. (13):

$$T^{\text{matter}} = T_{uu}du^2 + T_{vv}dv^2 + 2T_{uv}dudv + T_{ij}dx^i dx^j, \quad (23)$$

where the components T_{uu}, T_{uv}, T_{vv} , and T_{ij} are functions of u and v . This general form of the stress tensor will be used later as an ansatz in the backreacted shock wave geometry. Further, we assume that the metric given in Eq. (21) is a solution of the following Einstein equation:

$$R_{ab} - \frac{1}{2}g_{ab}R = 8\pi T_{ab}^{\text{matter}}, \quad (24)$$

where the form of the components T_{ab}^{matter} are given in Eq. (23). It is to be mentioned that the contribution coming from the cosmological constant has also been taken care by the part T_{ab}^{matter} [32]. Next, we consider that a tiny pulse of

energy E_0 is added to left side of the geometry from the boundary at an earlier time t . Considering $t = 0$ as the reference frame, the energy of the added perturbation (at earlier time t) gets blueshifted, and it follows an almost null trajectory toward the past horizon. This process introduces nontrivial modification to the original geometry [25,26]. Our motivation is to compute the change to the unperturbed geometry [given in Eq. (21)] and the associated stress tensor [given in Eq. (23)] due to the presence of the null pulse. In order to do this, we assume that the null pulse of energy is localized at $u = 0$, and it propagates along the v direction. In terms of the Penrose diagram, this consideration creates an extension along the v direction. Mathematically, this extension can be incorporated by considering the following transformations:

$$\begin{aligned} v &\rightarrow v + \theta(u)\alpha(t, x^i) \\ dv &\rightarrow dv + \theta(u)\partial_i\alpha(t, x^i)dx^i, \end{aligned} \quad (25)$$

where the form of the function $\alpha(t, x^i)$ is to be determined from the Einstein field equations. The theta function $\theta(u)$ ensures that the changes are constrained to the region $u > 0$ (left exterior). As mentioned earlier, the said nontrivial modification to the original spacetime can be understood with the help of a Penrose diagram. This we have given in Fig. 2. We now incorporate the transformations given in Eq. (25) to the unperturbed metric [given in Eq. (21)] and obtain the following form for the backreacted geometry:

$$\begin{aligned} ds^2 &= 2\Omega(u, v + \theta(u)\alpha(t, x^i))du(dv + \theta(u)\partial_i\alpha(t, x^i)dx^i) \\ &\quad + g_{ij}(u, v + \theta(u)\alpha(t, x^i))dx^i dx^j. \end{aligned} \quad (26)$$

For the sake of convenience, we now introduce the following set of new coordinates:

$$\begin{aligned} \bar{u} &= u \\ \bar{v} &= v + \theta(u)\alpha(t, x^i) \\ \bar{x}^i &= x^i. \end{aligned} \quad (27)$$

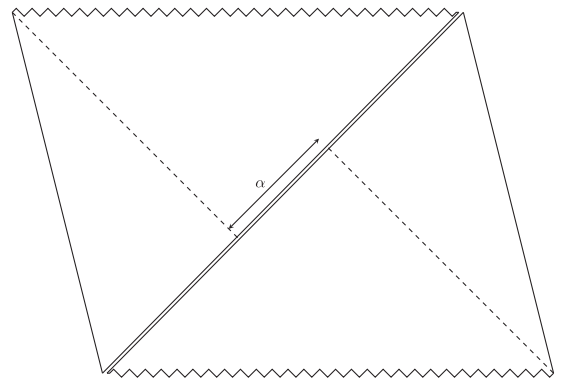


FIG. 2. Penrose diagram of the shock wave geometry.

From the above given coordinate transformations, one can easily show the following relation:

$$\begin{aligned} dv + \theta(u)\partial_i\alpha(t, x^i)dx^i &= d\bar{v} - \delta(u)\alpha(t, x^i)du \\ &= d\bar{v} - \delta(\bar{u})\alpha(t, \bar{x}^i)d\bar{u}. \end{aligned} \quad (28)$$

In terms of these new coordinates, the backreacted metric [given in Eq. (26)] takes the following form:

$$ds^2 = 2\Omega(\bar{u}, \bar{v})d\bar{u}[d\bar{v} - \delta(\bar{u})\alpha(t, \bar{x}^i)d\bar{u}] + g_{ij}(\bar{u}, \bar{v})d\bar{x}^i d\bar{x}^j. \quad (29)$$

In obtaining the above metric, we have used the relation given in Eq. (28). The above given metric is usually denoted as the general form of the shock wave metric. On the other hand, the general energy-momentum stress tensor corresponding to the matter part [given in Eq. (23)] is also modified as

$$\begin{aligned} T^{\text{matter}} &= [\bar{T}_{uu} - 2\delta(\bar{u})\alpha(t, \bar{x}^i)\bar{T}_{uv} + \delta^2(\bar{u})\alpha^2(t, \bar{x}^i)\bar{T}_{vv}]d\bar{u}^2 \\ &\quad + \bar{T}_{vv}d\bar{v}^2 + 2[\bar{T}_{uv} - \alpha(t, \bar{x}^i)\delta(\bar{u})\bar{T}_{vv}]d\bar{u}d\bar{v} \\ &\quad + \bar{T}_{ij}d\bar{x}^i d\bar{x}^j, \end{aligned} \quad (30)$$

where $T_{ab}(u, v + \theta(u)\alpha(t, x^i)) \equiv \bar{T}_{ab}$. Furthermore, the stress tensor associated to the shock wave is assumed to have the following form [4]:

$$T^{SW} = E_0 e^{\frac{2\pi}{\beta}t} \delta(\bar{u})d\bar{u}^2 \delta(\bar{x}^i), \quad (31)$$

where E_0 is the asymptotic energy of the null pulse, and $e^{\frac{2\pi}{\beta}t}$ is the blue shift factor. Further $\delta(\bar{x}^i)$ ensures that the perturbation is localized at $x^i = 0$. In order to find the profile of $\alpha(t, \bar{x}^i)$, we assume that the perturbed metric [given in Eq. (29)] is a valid solution of the following Einstein equation:

$$R_{ab} - \frac{1}{2}g_{ab}R = 8\pi(T_{ab}^{\text{matter}} + T_{ab}^{SW}), \quad (32)$$

where the expressions of T_{ab}^{matter} and T_{ab}^{SW} are given in Eqs. (30) and (31) respectively. For the sake of simplicity, we now introduce a bookkeeping parameter ϵ in $\alpha(t, \bar{x}^i)$ as, $\alpha(t, \bar{x}^i) \rightarrow \epsilon\alpha(t, \bar{x}^i)$ and T_{ab}^{SW} as $T_{ab}^{SW} \rightarrow \epsilon T_{ab}^{SW}$, where $|\epsilon| \ll 1$. This process helps us in recovering the unperturbed Einstein equation [given in Eq. (24)] in the limit $\epsilon \rightarrow 0$.

Firstly, we solve the unperturbed Einstein field equation [given in Eq. (24)] in order to obtain the values of T_{uu} , T_{vv} , and T_{uv} . We then substitute these values in the uu component of the perturbed Einstein field equation given in Eq. (32) and keep terms up to $\sim \mathcal{O}(\epsilon)$. We then observe that the shock wave parameter $\alpha(t, \bar{x}^i)$ satisfies the following equation (on the horizon $u = 0$ or $r = r_+$):

$$\delta(\bar{u})g^{ij} \left[\Omega(\bar{u}, \bar{v})\partial_i\partial_j - \frac{1}{2}g_{ij,\bar{u}\bar{v}} \right] \alpha(t, \bar{x}^i) = 8\pi T_{uu}^{SW}. \quad (33)$$

The above equation can be obtained from the uu component of the perturbed Einstein equation [given in Eq. (32)]. We would like to mention that in obtaining the above equation, the following conditions must hold [26,29]:

$$\Omega(\bar{u}, \bar{v})_{,\bar{v}} = g_{ij,\bar{v}} = T_{vv}^{\text{matter}} = 0 \quad \text{at } \bar{u} = 0. \quad (34)$$

We now proceed to express Eq. (33) in terms of the t and r coordinates in which the background spacetime [Eq. (13)] was initially expressed. Furthermore, one needs to keep in mind the fact that Eq. (33) is to be evaluated on the horizon $\bar{u} = 0$ or $r = r_+$. This motivates us to consider the following near-horizon expansion of the black hole lapse function $\xi(r) \equiv r^{2p}f(r)$:

$$\begin{aligned} \xi(r) &= \xi(r_+) + \partial_r \xi(r)|_{r=r_+}(r - r_+) + \dots \\ &= cr_+^{2p-1}(r - r_+) + \dots \end{aligned} \quad (35)$$

In the above computation we have used the fact that $f(r)|_{r=r_+} = 0$. By using the above near-horizon form, one can show that the Tortoise coordinate takes the following form:

$$r_* \approx \left(\frac{1}{cr_+^{2p-1}} \right) \ln \left(\frac{r - r_+}{r_+} \right). \quad (36)$$

Further, the expression of uv is obtained to be in the near-horizon limit

$$uv = e^{\frac{4\pi}{\beta}r_*} \approx e^{\ln \left(\frac{r-r_+}{r_+} \right)}. \quad (37)$$

We now make use of the above near-horizon expressions to compute the expression of $\Omega(\bar{u}, \bar{v})$ and $g_{ij,\bar{u}\bar{v}}$ on the horizon $\bar{u} = 0$ which appears in Eq. (33). This reads as

$$\begin{aligned} \Omega(\bar{u}, \bar{v})|_{\bar{u}=0} &= \frac{\beta^2 r^{2p} f(r)}{8\pi^2 uv} \Big|_{\bar{u}=0} \\ &\approx \frac{1}{2} \left(\frac{2}{cr_+^{2p-1}} \right)^2 cr_+^{2p-1} (r - r_+) e^{-\ln \left(\frac{r-r_+}{r_+} \right)} + \dots \\ &\approx \frac{2}{cr_+^{2p-2}} \equiv \Omega(r_+). \end{aligned} \quad (38)$$

In the above computation, we have used the near-horizon expansions given in Eqs. (35) and (36). We now proceed to compute $\frac{1}{2} \frac{dg_{ij}}{d(\bar{u}\bar{v})} \Big|_{\bar{u}=0}$. This reads as

$$\begin{aligned} \frac{dg_{ij}}{d(\bar{u}\bar{v})} \Big|_{\bar{u}=0} &= \left(\frac{dg_{ij}}{dr_*} \right) \left(\frac{dr_*}{d(\bar{u}\bar{v})} \right) \Big|_{\bar{u}=0} \\ &= r^{2p} f(r) \frac{\beta}{4\pi} e^{\frac{4\pi r_*}{\beta}} \partial_r g_{ij} \Big|_{r=r_+}, \end{aligned} \quad (39)$$

where $\beta = \frac{4\pi}{cr_+^{2p-1}}$ is the inverse Hawking temperature. Next, we use the near-horizon expansions given in Eqs. (35) and (36) in the above expression. This in turn gives us

$$\begin{aligned} \left. \frac{dg_{ij}}{d(\bar{u} \bar{v})} \right|_{\bar{u}=0} &\approx (cr_+^{2p-1}) \left(\frac{r-r_+}{cr_+^{2p-1}} \right) e^{-\ln(\frac{r-r_+}{r_+})} \partial_r g_{ij} \Big|_{r=r_+} \\ &= r_+ \partial_r g_{ij} \Big|_{r=r_+}. \end{aligned} \quad (40)$$

For the sake of simplicity, we have denoted $r_+ \partial_r g_{ij} \Big|_{r=r_+}$ as $r_+ \partial_r g_{ij}(r_+)$.

By using the above results in Eq. (33), we obtain the following form:

$$g^{ij}(r_+) \left[\Omega(r_+) \partial_i \partial_j - \frac{r_+}{2} \partial_r g_{ij}(r_+) \right] \alpha(t, x^i) = 8\pi E_0 e^{\frac{2\pi}{\beta} t} \delta(\bar{x}^i). \quad (41)$$

We now choose the direction of propagation for the perturbation as $x^i = x_1$. This further simplifies the Eq. (41) to the following form:

$$[\partial_{x_1}^2 - M^2] \alpha(t, x_1) = E_0 e^{\frac{2\pi}{\beta}(t-t_*)} \delta(\bar{x}^i), \quad (42)$$

where

$$\begin{aligned} M^2 &= \frac{(d-1)r_+}{2\Omega(r_+)} \partial_r g_{x_1 x_1}(r_+), \\ t_* &= \left(\frac{\beta}{2\pi} \right) \log \left(\frac{\Omega(r_+)}{8\pi g_{x_1 x_1}(r_+)} \right). \end{aligned} \quad (43)$$

We now make use of the metric given in Eq. (13) along with Eq. (38) and the fact that $g_{x_1 x_1}(r_+) = r_+^{2p}$ in order to obtain explicit expressions for M^2 and t_* . These read as

$$M^2 = \frac{c}{2} p(d-1) r_+^{2(2p-1)} \quad (44)$$

$$t_* = \left(\frac{\beta}{2\pi} \right) \log \left(\frac{r_+^{p(d-1)}}{4\pi c r_+^{p(d+2)-2}} \right). \quad (45)$$

In the above expression, t_* represents the scrambling time which can be recast to the following standard form:

$$t_* \approx \left(\frac{\beta}{2\pi} \right) \log(S_{\text{BH}}), \quad (46)$$

where S_{BH} is the Bekenstein-Hawking entropy density of the nonconformal black brane which has the form

$$S_{\text{BH}} = \frac{r_+^{p(d-1)}}{4}. \quad (47)$$

We now proceed to solve Eq. (42). For $|x_1| \neq 0$, the solution for $\alpha(t, x_1)$ reads as

$$\alpha(t, x_1) = \begin{cases} c_0 e^{Mx_1}; & \text{for } x < 0 \\ c_1 e^{-Mx_1}; & \text{for } x > 0. \end{cases} \quad (48)$$

The above solution for both the regions must be continuous at $x = 0$ which gives the condition $c_0 = c_1$. On the other hand, by integrating Eq. (42) one obtains

$$\begin{aligned} \lim_{\epsilon \rightarrow 0} \left[\int_{x_1=0-\epsilon}^{x_1=0+\epsilon} (\partial_{x_1}^2 - M^2) \alpha(t, x_1) dx_1 \right] \\ = E_0 e^{\frac{2\pi}{\beta}(t-t_*)} \lim_{\epsilon \rightarrow 0} \left[\int_{x_1=0-\epsilon}^{x_1=0+\epsilon} \delta(x_1) dx_1 \right] \\ \Rightarrow \lim_{\epsilon \rightarrow 0} [\partial_{x_1} \alpha(t, x_1)|_{x_1=0+\epsilon} - \partial_{x_1} \alpha(t, x_1)|_{x_1=0-\epsilon}] \\ = E_0 e^{\frac{2\pi}{\beta}(t-t_*)}. \end{aligned} \quad (49)$$

We now make use of the solution given in Eq. (48) in the above equation which in turn gives

$$c_0 + c_1 = \frac{E_0}{M} e^{\frac{2\pi}{\beta}(t-t_*)}. \quad (50)$$

By using the condition $c_0 = c_1$ along with Eq. (50), we obtain the solution for Eq. (42) to be

$$\begin{aligned} \alpha(t, x_1) &= \frac{E_0}{2M} e^{\frac{2\pi}{\beta}(t-t_*) - M|x_1|} \\ &\sim \text{constant} \times e^{\frac{2\pi}{\beta}(t-t_*) - M|x_1|}. \end{aligned} \quad (51)$$

A few comments are in order now. Keeping in mind Eq. (2), it is to be noted that the difference between states created by $\hat{W}(x, t) \hat{V}(0)$ and $\hat{V}(0) \hat{W}(x, t)$ is related to the null shift of the operator $\hat{V}(0)$ created by the shock wave profile $\alpha(x, t)$. As the commutator $\langle [\hat{W}(x, t), \hat{V}(0)]^2 \rangle_\beta$ is determined by the real part of $\langle \hat{W}(x, t) \hat{V}(0) \hat{W}(x, t) \hat{V}(0) \rangle_\beta$ [8,88], at early times $\beta < t < t_* + \frac{x}{v_B}$, one has [5,8,88]

$$\mathcal{C}(t, x) \sim \alpha(t, x). \quad (52)$$

We now compute the expressions for the Lyapunov exponent and butterfly velocity by comparing the above with Eq. (3). This yields the following results:

$$\lambda_L = \frac{2\pi}{\beta}; \quad v_B = \frac{1}{4} \sqrt{\frac{8d}{d-1} - \eta^2}, \quad (53)$$

where the expression for β is given in Eq. (15). In the conformal limit $\eta \rightarrow 0$, one obtains $\beta = \frac{dr_+}{4\pi}$ and $v_B = \sqrt{\frac{d}{2(d-1)}}$. This in turn means that in this particular limit one recovers the SAdS $_{d+1}$ results given in [4].

We would now like to make a few comments regarding our results. It can be observed that the form of the Lyapunov exponent remains unchanged, that is, $\lambda_L = 2\pi T_H$, and this form is universal for any maximally chaotic holographic theory. Further, it also depicts the fact that the Lyapunov exponent depends only on the Hawking temperature T_H (which is also the temperature of the dual field theory). However, the Hawking temperature is subject to the holographic model under consideration which in our case corresponds to the nonconformal black brane solution. Here, the parameter η in the gravitational solution characterizes the theory since it appears in the bulk action [Eq. (11)]. From the perspective of the dual theory, η corresponds to turning on some deformation away from conformality, which implies choosing a particular boundary theory. Once η is chosen, we would then fix β , which characterizes the thermal state of the dual field theory, to make plots of the various quantities that we shall compute in the subsequent sections. From Fig. 3 we observe that an increase in the value of the parameter η decreases the value of the butterfly velocity v_B and finally for $\eta = \sqrt{\frac{8d}{d-1}}$ it vanishes. This implies that due to the presence of non-conformality, the speed of information spreading (v_B) in the system gets decreased representing the delay in the growth of the initial perturbation provided to the system. For $\eta = \sqrt{\frac{8d}{d-1}}$, the system attains something known as the Lyapunov stability as for this particular value of η , the Hawking temperature of the nonconformal black brane is zero which in turn gives us a vanishing Lyapunov exponent, that is, $\lambda_L = 0$. This can also be understood as the steady state. In this case, the signature of chaos in the system vanishes, and the system becomes conservative. As a consequence of the Lyapunov stability, the butterfly effect also vanishes which is being manifested here as $v_B = 0$ [2]. We have already mentioned that this particular value of $\eta = \sqrt{\frac{8d}{d-1}}$ has the interpretation of being the upper bound (Gubser bound) of η [83,84]. The physics behind the Gubser bound is the following. For the Einstein-dilaton

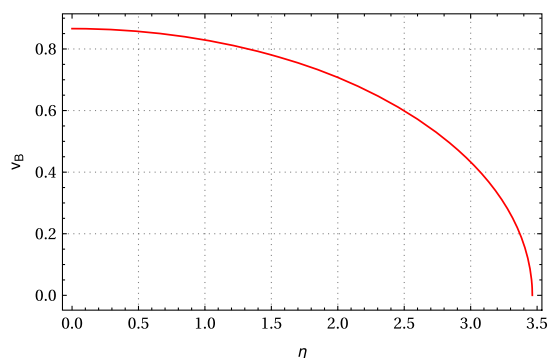


FIG. 3. Variation of the butterfly velocity (v_B) with respect to the nonconformal parameter η , where we set $d = 3$.

black brane geometry to be thermodynamically stable, η^2 should always be less than $\frac{8d}{d-1}$. This value is known as the Gubser bound. When η^2 exceeds this value, the Einstein-dilaton black brane and its dual theory are unstable thermodynamically [78,80]. It can also be seen from the solution for $f(r)$ [Eq. (13)] that c becomes negative when η^2 exceeds the Gubser bound. So $\eta^2 \leq \frac{8d}{d-1}$ for c to be positive. From our obtained results, we also confirm this observation from the point of view of chaos, as for $\eta < \sqrt{\frac{8d}{d-1}}$, the system is chaotic as both λ_L and v_B are positive and for $\eta = \sqrt{\frac{8d}{d-1}}$, the system is conservative. One can also recast the expressions given in Eq. (53) to the following forms:

$$\begin{aligned} \lambda_L &= \lambda_L^{(c)} \left(\frac{\beta^{(c)}}{\beta} \right) \\ v_B &= v_B^{(c)} \sqrt{\left[1 - \frac{(d-1)\eta^2}{8d} \right]}. \end{aligned} \quad (54)$$

The above forms help us to point out the nonconformal corrections to the conformal results. Here, $\lambda_L^{(c)}$, $\beta^{(c)}$, and $v_B^{(c)} = \sqrt{\frac{d}{2(d-1)}}$ correspond to the Lyapunov exponent, inverse Hawking temperature, and butterfly velocity for the SAdS $_{d+1}$ black brane. As one shall have the SAdS $_{d+1}$ black brane solution in the conformal limit $\eta \rightarrow 0$, we denote the corresponding results as conformal results [that is why we use the superscript (c)].

IV. TWO-SIDED HTMI AND ENTANGLEMENT VELOCITY

In this section, we compute the HTMI between the two decoupled quantum mechanical systems existing on both left and right asymptotic boundaries of the two-sided black hole geometry [21]. Further, we do this for both unperturbed and perturbed geometries in order to quantify the effect of shock wave on HTMI.

A. HTMI for the unperturbed Einstein-dilaton black brane geometry

First, we holographically compute the two-sided thermomutual information in absence of the shock wave. In order to do this, we consider two striplike, identical subsystems of length l , namely, A and B which belong to the left and right asymptotic boundaries respectively. The geometry of these striplike subsystems (A and B) can be specified as $-\frac{l}{2} \leq x_1 \leq \frac{l}{2}$ and $-\frac{l}{2} \leq x_m \leq \frac{l}{2}$ for $m = 2, \dots, d-1$. As mentioned previously, the expression for HTMI is given by Eq. (5). To calculate this, one needs to compute the von Neumann entropies associated to subsystem A , B and $A \cup B$. In the gauge/gravity setup, one can

holographically do this by incorporating the RT proposal [89–91] which states that the von Neumann entropy of a subsystem (for example A) can be computed with the help of the extremal surface with minimal area γ_A . By incorporating this proposal, one can obtain the following result [85]:

$$S_{\text{vn}}(A) = S_{\text{vn}}(B) = \frac{2L^{d-2}}{4} \int_{r_t}^{\infty} \frac{r^{p(d-3)} dr}{\sqrt{f(r)} \sqrt{1 - \left(\frac{r}{r_t}\right)^{2p(d-1)}}}, \quad (55)$$

where r_t is the turning point of the static minimal surface of interest. On the other hand, the relation between the subsystem size l and the turning point r_t stands to be

$$l = 2 \int_{r_t}^{\infty} \frac{dr}{r^{2p} \sqrt{f(r)} \sqrt{\left(\frac{r}{r_t}\right)^{2p} - 1}}. \quad (56)$$

The computation of $S_{\text{vn}}(A \cup B)$ is tricky. For this, one proceeds with the surface $\gamma_{\text{wormhole}} = \gamma_1 \cup \gamma_2$ which bifurcates the event horizon in order to connect the asymptotic boundaries of the two-sided eternal black hole spacetime. This is basically a nontraversable wormhole geometry which induces entanglement between the two decoupled theories (at right and left asymptotic boundaries of the spacetime geometry). It is to be noted that γ_1 corresponds to the $x_1 = -\frac{l}{2}$ hyperplane and γ_2 corresponds to the $x_1 = \frac{l}{2}$ hyperplane. If we consider the area of a single surface (with such properties), then symmetry tells us that the total area will be four times the area of the single surface. A graphical representation of the setup has been shown in Fig. 4. This leads to the following expression:

$$S_{\text{vn}}(A \cup B; \alpha = 0) \equiv \frac{\text{Area}(\gamma_{\text{wormhole}})}{4} = \frac{4L^{d-2}}{4} \int_{r_+}^{\infty} \frac{r^{p(d-3)} dr}{\sqrt{f(r)}}. \quad (57)$$

We now substitute the expressions from Eqs. (55) and (57) in Eq. (5) and obtain the following form of the two-sided HTMI (in the absence of shock wave):

$$I(A; B; \alpha = 0) = L^{d-2} \left[\int_{r_t}^{\infty} \frac{r^{p(d-3)} dr}{\sqrt{f(r)} \sqrt{1 - \left(\frac{r}{r_t}\right)^{2p(d-1)}}} - \int_{r_+}^{\infty} \frac{r^{p(d-3)} dr}{\sqrt{f(r)}} \right]. \quad (58)$$

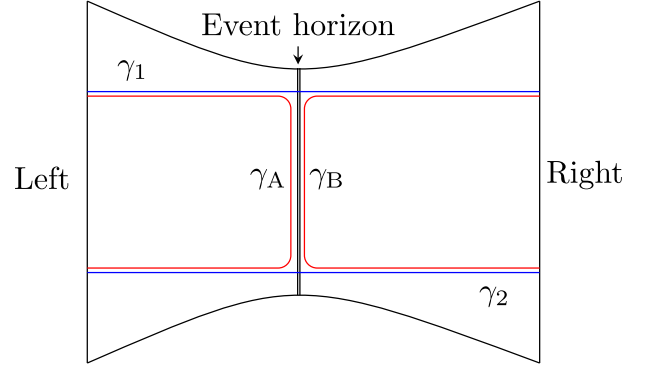


FIG. 4. Schematic representation of the two-sided eternal black hole geometry in the absence of the shock wave. Here, γ_A and γ_B (in red) are Ryu-Takayanagi surfaces associated to the subsystems A and B . γ_1 and γ_2 (in blue) lead to the extremal surface $\gamma_{\text{wormhole}} = \gamma_1 \cup \gamma_2$ which connects the two decoupled boundaries (right and left).

The above expression represents the mutual correlation between the two decoupled theories living at the right and left asymptotic boundaries of the two-sided nonconformal black brane geometry [given in Eq. (13)]. It can be seen that the expression is written in terms of the bulk coordinate r and one can represent it in terms of the boundary coordinate (subsystem size l) with the help of Eq. (56).

B. HTMI for the shock wave geometry

We now proceed to compute the expression of $I(A; B)$ in the presence of the shock wave modification of the original geometry. In order to do this, we follow the computational procedure shown in [27]. In this work, we are considering a homogeneous shock wave which is introducing deformation on the horizon along the v coordinate which in turn stretches the wormhole geometry. We denote this new elongated wormhole geometry as $\gamma_{\text{wormhole}}^{\text{SW}} = \gamma_1 \cup \gamma_2$. This leads to the fact that only the term $S_{\text{vn}}(A; B)$ gets affected due to the presence of the shock wave as it is the only term in Eq. (5) which depends on the wormhole geometry. A nice review related to this topic can be found in [92]. $S_{\text{vn}}(A)$ and $S_{\text{vn}}(B)$ remain unchanged as their associated extremal surfaces do not bifurcate the event horizon [93]. This can be graphically represented by a schematic diagram which has been provided in Fig. 5. Keeping this in mind, for the shock wave geometry, one can write down the following expression:

$$\begin{aligned} I(A; B; \alpha) &= S_{\text{vn}}(A) + S_{\text{vn}}(B) - S_{\text{vn}}(A \cup B; \alpha) \\ &= S_{\text{vn}}(A) + S_{\text{vn}}(B) - S_{\text{vn}}(A \cup B; \alpha = 0) \\ &\quad - [S_{\text{vn}}(A \cup B; \alpha) - S_{\text{vn}}(A \cup B; \alpha = 0)] \\ &= I(A; B; \alpha = 0) - S_{\text{vn}}^{\text{reg}}(A \cup B; \alpha), \end{aligned} \quad (59)$$

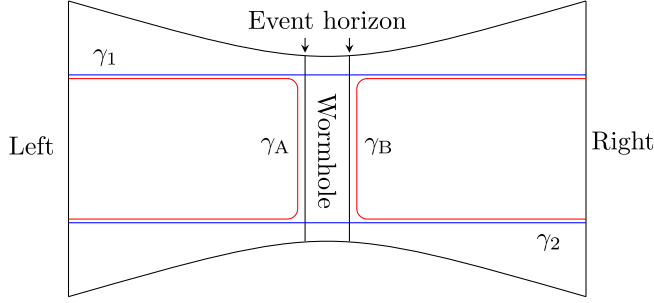


FIG. 5. Schematic representation of the shock wave geometry. In presence of the shock wave, only the extremal surface $\gamma_{\text{wormhole}}^{\text{SW}} = \gamma_1 \cup \gamma_2$ (in blue) is getting affected.

where $I(A:B;\alpha=0)$ is given in Eq. (58) and $S_{\text{vn}}^{\text{reg}}(A \cup B;\alpha)$ represents a regularized expression for the von Neumann entropy which is free of the universal divergence term.

Furthermore, in the above computation we have also introduced $S_{\text{vn}}(A \cup B;\alpha=0)$, which we have already computed in Eq. (57). The expression given in Eq. (59) in turn means that we need to compute only the term $S_{\text{vn}}^{\text{reg}}(A \cup B;\alpha)$. In order to compute $S_{\text{vn}}(A \cup B;\alpha)$ we first specify the parametrization of the corresponding Hubeny-Ryu-Takayanagi (HRT) surfaces $r = r(t)$, $x_1 = \pm \frac{l}{2}$, and $-\frac{l}{2} \leq x_m \leq \frac{l}{2}$ for $m = 2, \dots, d-1$. This leads to the corresponding area functional,

$$\text{Area}(\gamma_{\text{wormhole}}^{\text{SW}}) = L^{d-2} \int r^{p(d-1)} \sqrt{-f(r) + \frac{\dot{r}^2}{r^{4p}f(r)}} dt. \quad (60)$$

It is to be noted that the above area functional for the wormhole has been computed by using the original geometry. However, unlike the unperturbed scenario [given in Eq. (57)], one has to make use of the HRT proposal for the computation as the time-dependent shock wave perturbation makes the bulk direction time dependent, that is, $r = r(t)$, and introduces time-dependent modification to the wormhole geometry [27] (see Fig. 5):

$$\gamma_{\text{wormhole}} \xrightarrow{\alpha(t, x_1)} \gamma_{\text{wormhole}}^{\text{SW}}. \quad (61)$$

The Lagrangian density can be read off from the above action and has the form

$$\mathcal{L}(r, \dot{r}, t) = L^{d-2} r^{p(d-1)} \sqrt{-f(r) + \frac{\dot{r}^2}{r^{4p}f(r)}}. \quad (62)$$

The corresponding Hamiltonian density can easily be obtained from the definition

$$\mathcal{H}(r, p_r, t) = p_r \dot{r} - \mathcal{L}; \quad p_r = \frac{\partial \mathcal{L}}{\partial \dot{r}}. \quad (63)$$

This in turn gives

$$\mathcal{H}(r, p_r) = r^{p(d-1)} \frac{f(r)}{\sqrt{-f(r) + \frac{\dot{r}^2}{r^{4p}f(r)}}}, \quad (64)$$

where it can be observed that the Hamiltonian $\mathcal{H}(r, p_r)$ does not have an explicit dependency on time t . Hence, the Hamiltonian is a constant of motion. This can be written down as

$$\mathcal{H}(r, p_r) = \mathcal{C} \equiv \text{constant}, \quad (65)$$

where the conserved quantity \mathcal{C} can be evaluated at the point $r = r_0$ where $\dot{r}|_{r=r_0} = 0$. This reads as

$$\mathcal{C} = \mathcal{H}|_{r=r_0} \equiv -r_0^{p(d-1)} \sqrt{-f(r_0)}. \quad (66)$$

The on shell area functional therefore reads as

$$\text{Area}(\gamma_{\text{wormhole}}^{\text{SW}}) = L^{d-1} \int \frac{r^{p(d-3)} dr}{\sqrt{f(r) - \left(\frac{r_0}{r}\right)^{2p(d-1)} f(r_0)}}. \quad (67)$$

On the other hand, the time coordinate can be represented in the following way:

$$t(r) = \pm \int \frac{dr}{r^{2p} f(r) \sqrt{1 - \left(\frac{r_0}{r}\right)^{2p(d-1)} \frac{f(r)}{f(r_0)}}}. \quad (68)$$

We now proceed to specify the domain of integration for the above expressions. The domain of interest can be divided into three segments which has been pointed out in Fig. 6. It can be observed that segment II and segment III have the same area. Keeping these observations in mind, we write down the following form:

$$S_{\text{vn}}(A \cup B;\alpha) = \frac{4L^{d-2}}{4} \left[\int_{r_+}^{\infty} \frac{r^{p(d-3)} dr}{\sqrt{f(r) - \left(\frac{r_0}{r}\right)^{2p(d-1)} f(r_0)}} + 2 \int_{r_0}^{r_+} \frac{r^{p(d-3)} dr}{\sqrt{f(r) - \left(\frac{r_0}{r}\right)^{2p(d-1)} f(r_0)}} \right]. \quad (69)$$

With the above result in hand, we now make use of the expression for $S_{\text{vn}}(A \cup B;\alpha=0)$ [given in Eq. (57)] in order to obtain the regularized version of $S_{\text{vn}}(A \cup B;\alpha)$.

This reads as

$$S_{\text{vn}}^{\text{reg}}(A \cup B; \alpha) = S_{\text{vn}}(A \cup B; \alpha) - S_{\text{vn}}(A \cup B; \alpha = 0) \\ = \frac{4L^{d-2}}{4} \left[\int_{r_+}^{\infty} r^{p(d-3)} \left(\frac{1}{\sqrt{f(r) - \left(\frac{r_0}{r}\right)^{2p(d-1)} f(r_0)}} - \frac{1}{\sqrt{f(r)}} \right) dr + 2 \int_{r_0}^{r_+} \frac{r^{p(d-3)} dr}{\sqrt{f(r) - \left(\frac{r_0}{r}\right)^{2p(d-1)} f(r_0)}} \right]. \quad (70)$$

As we have explained in Eq. (59), the above expression of $S_{\text{vn}}^{\text{reg}}(A \cup B; \alpha)$ along with the expression of $I(A; B; \alpha = 0)$ [given in Eq. (58)] leads us to the desired result of $I(A; B; \alpha)$. It is to be observed from the above expression of $S_{\text{vn}}^{\text{reg}}(A \cup B; \alpha)$ that it is a function of r_0 . Before we proceed further we would like to make few comments. From Eq. (70) one can observe that in the limit $r_0 \rightarrow r_+$, $S_{\text{vn}}(A \cup B; \alpha) = S_{\text{vn}}(A \cup B; \alpha = 0)$. We would like to point out that the emergence of the point r_0 in the black hole interior (see Fig. 6) is precisely due to the shock wave perturbation of the original geometry. This in turn means that we need to find the relation between α (the shock wave parameter) and r_0 so that we can depict the variation of $S_{\text{vn}}^{\text{reg}}(A \cup B; \alpha)$ with respect to the shock wave parameter. In order to do this, we follow the approach given in [27]. As we have mentioned earlier, our domain of interest can be divided into three segments, namely, I, II, and III. This precise partitioning of the concerned region is solely due to the presence of the shock wave. In terms of the Kruskal coordinates, segment I connects $(u, v) = (1, -1)$ (boundary) to $(u, v) = (u_1, 0)$ (horizon). Segment II connects $(u, v) = (u_1, 0)$ (horizon) to the point r_0 which is at $(u, v) = (u_2, v_2)$, and segment III connects the point r_0 , that is, $(u, v) = (u_2, v_2)$ to

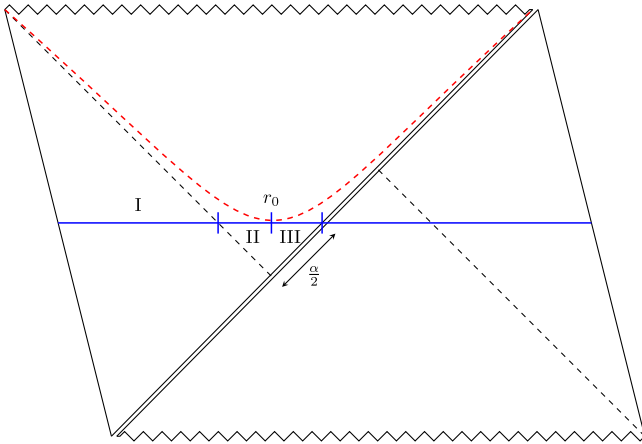


FIG. 6. Deformation of the extremal surface $\gamma_{\text{wormhole}}^{\text{SW}}$ (in blue) due to the shock wave. We have divided the left half of the surface into three parts, segment I which spans from the boundary ($r = \infty$) to the horizon r_+ , and both segment II and segment III spans from r_0 to the horizon r_+ . Thus, segment II and segment III have same area.

$(u, v) = (0, \alpha/2)$. Keeping these coordinates in mind and by using the Kruskal coordinates, one can show the following relations:

$$u_1^2 = \exp \left(\frac{4\pi}{\beta} \int_{r_+}^{\infty} \frac{dr}{r^{2p} f(r)} \left[\frac{1}{\sqrt{1 - \left(\frac{r}{r_0}\right)^{2p(d-1)} \frac{f(r)}{f(r_0)}}} - 1 \right] \right), \\ u_2^2 = \exp \left(\frac{4\pi}{\beta} \int_{r_0}^{r_+} \frac{dr}{r^{2p} f(r)} \left[\frac{1}{\sqrt{1 - \left(\frac{r}{r_0}\right)^{2p(d-1)} \frac{f(r)}{f(r_0)}}} - 1 \right] \right), \\ v_2 = \frac{1}{u_2} \exp \left(-\frac{4\pi}{\beta} \int_{r_0}^{\bar{r}} \frac{dr}{r^{2p} f(r)} \right). \quad (71)$$

In the last of the above equations, the \bar{r} point resides inside the horizon at which $r_* = 0$. From segment III, one can show the following relation by incorporating the variation in the v coordinate:

$$\frac{\alpha^2}{4v_2^2} = \exp \left(\frac{4\pi}{\beta} \int_{r_+}^{r_0} \frac{dr}{r^{2p} f(r)} \left[\frac{1}{\sqrt{1 - \left(\frac{r}{r_0}\right)^{2p(d-1)} \frac{f(r)}{f(r_0)}}} - 1 \right] \right) \\ = \frac{u_1^2}{u_2^2}. \quad (72)$$

Now by using the relation given by Eq. (71) in the above equation and after some simplifications, one obtains the following relation:

$$\alpha(r_0) = 2 \exp(\xi_I + \xi_{II} + \xi_{III}), \quad (73)$$

where

$$\xi_I = \frac{4\pi}{\beta} \int_{\bar{r}}^{r_0} \frac{dr}{r^{2p} f(r)} \\ \xi_{II} = \frac{2\pi}{\beta} \int_{r_+}^{\infty} \frac{dr}{r^{2p} f(r)} \left[1 - \frac{1}{\sqrt{1 - \left(\frac{r}{r_0}\right)^{2p(d-1)} \frac{f(r)}{f(r_0)}}} \right] \\ \xi_{III} = \frac{4\pi}{\beta} \int_{r_0}^{r_+} \frac{dr}{r^{2p} f(r)} \left[1 - \frac{1}{\sqrt{1 - \left(\frac{r}{r_0}\right)^{2p(d-1)} \frac{f(r)}{f(r_0)}}} \right]. \quad (74)$$

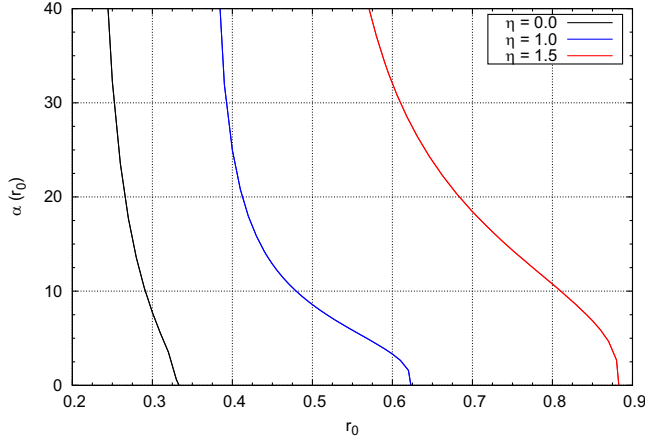


FIG. 7. Behavior of the shock wave parameter $\alpha(r_0)$ with respect to the turning point r_0 . We have set $\beta = 4\pi$ and $d = 3$. Here, the right curve is for $\eta = 1.5$, the middle curve is for $\eta = 1.0$, and the left curve is for $\eta = 0.0$.

In Fig. 7, we have graphically represented the relation given in Eq. (73) with $\beta = 4\pi$. We observe that $\alpha(r_0)$ decreases with the increase in the value of the r_0 and ultimately vanishes at $r_0 = r_+$. The lesson that one can learn from this observation is the following. For a fixed β , an increase in the value of the nonconformal parameter η increases the value of r_+ . This can be understood from the relation provided in Eq. (16). This in turn means that the presence of nonconformality leads to a higher value of r_0 at which the shock wave parameter vanishes. It is also to be noted that for a critical value of r_0 , namely, at $r_0 = r_c$ the shock wave parameter $\alpha(r_0)$ diverges. In fact, it can also be observed that at this particular value $r_0 = r_c$, only ξ_{III} diverges which depicts the fact that in the limit $r_0 \rightarrow r_c$, ξ_{III} is the dominating piece in the expression of $\alpha(r_0)$ [given in Eq. (73)]. One can derive the value of r_c by performing a Taylor expansion of the integrand of ξ_{III} around $r_0 \approx r_c$ and equating the coefficient of $(r_0 - r_c)$ to zero [29,31,32]. We shall follow this approach to derive the explicit expression of r_c . Firstly, the expression of ξ_{III} around $r \approx r_0$ has the following form:

$$\xi_{\text{III}} \approx \frac{4\pi}{\beta} \int_{r_0}^{r_+} \frac{dr}{r_0^{2p} f(r_0)} \left[1 - \frac{1}{\sqrt{\left(-\frac{2p(d-1)}{r_0} - \frac{f'(r_0)}{f(r_0)} \right) (r - r_0)}} \right]. \quad (75)$$

The above expression diverges at

$$-\frac{2p(d-1)}{r_0} - \frac{f'(r_0)}{f(r_0)} \Big|_{r_0=r_c} = 0.$$

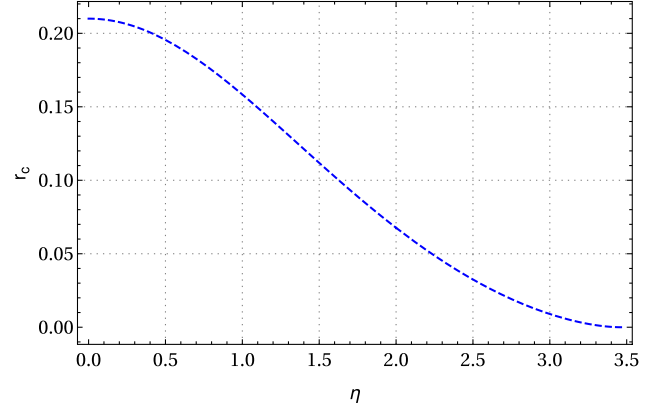


FIG. 8. Effect of the nonconformal parameter η on r_c . We have set $d = 3$ and $\beta = 4\pi$.

By solving this one obtains

$$r_c = r_+ \left[1 - \frac{c}{2p(d-1)} \right]^{\frac{1}{c}}. \quad (76)$$

In the limit $\eta \rightarrow 0$, one obtains the conformal result [27]

$$r_c = r_+ \left[\frac{d-2}{2(d-1)} \right]^{\frac{1}{d}}. \quad (77)$$

We now make use of the relation given in Eq. (16) in order to recast the expression of r_c [given in Eq. (76)] to the following form:

$$r_c = \left(\frac{\beta c}{4\pi} \right)^{\frac{1}{1-2p}} \left[1 - \frac{c}{2p(d-1)} \right]^{\frac{1}{c}}. \quad (78)$$

In Fig. 8, we have graphically represented the above expression of r_c for a fixed value of β in order to capture the effect of nonconformality on it. We observe that nonconformality decreases the value of r_c which implies the fact that nonconformality helps to probe the black hole interior further. In Fig. 9, the behavior of $S_{\text{vn}}^{\text{reg}}(A \cup B; \alpha)$ and $\frac{I(A:B;\alpha)}{I(A:B;\alpha=0)} = 1 - \frac{S_{\text{vn}}^{\text{reg}}(A \cup B; \alpha)}{I(A:B;\alpha=0)}$ with respect to the logarithm of the shock wave parameter ($\log \alpha$) has been provided. We observe that for a fixed value of $\log \alpha$, $S_{\text{vn}}^{\text{reg}}(A \cup B; \alpha)$ increases with the increase in the value of the nonconformal parameter η . On the other hand, due to nonconformality, $S_{\text{vn}}^{\text{reg}}(A \cup B; \alpha)$ becomes equal to $I(A:B; \alpha = 0)$ (resulting in $\frac{I(A:B;\alpha)}{I(A:B;\alpha=0)} = 0$) for a smaller value of $\log \alpha$.

C. Entanglement velocity

We now proceed to study the behavior of $S_{\text{vn}}^{\text{reg}}(A \cup B; \alpha)$ with respect to the time t at which the initial perturbation was added. It can be observed that $S_{\text{vn}}^{\text{reg}}(A \cup B; \alpha)$ grows linearly with respect to $\log \alpha$ which in turn means it grows

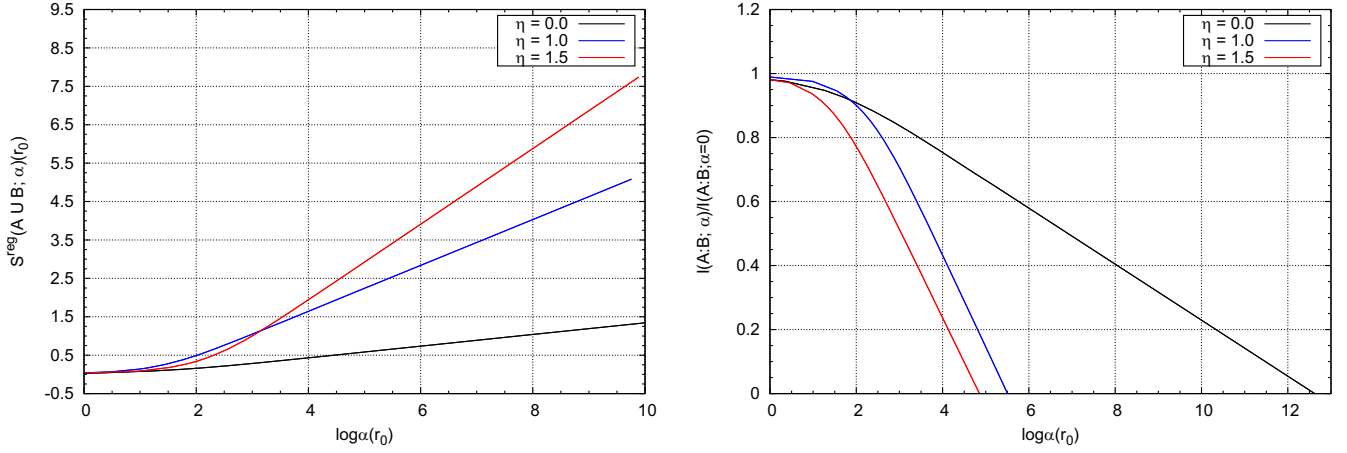


FIG. 9. The left plot represents the behavior of $S_{\text{vn}}^{\text{reg}}(A \cup B; \alpha)$ with respect to $\log \alpha$. The right plot captures the behavior of the thermomutual information in the presence of the shock wave. Here, we have set $\beta = 4\pi$, $L = 1$ and $d = 3$. Left plot: the upper curve is for $\eta = 1.5$, the middle curve is for $\eta = 1.0$ and the lower curve is for $\eta = 0.0$. Right plot: the upper curve is for $\eta = 0.0$, the middle curve is for $\eta = 1.0$ and the lower curve is for $\eta = 1.5$.

linearly with respect to t (as $\alpha \approx e^{\frac{2\pi}{\beta}t}$). This can be observed from the left plot of Fig. 9. This linear behavior of $S_{\text{vn}}^{\text{reg}}(A \cup B; \alpha)$ in turn helps us to quantify the spreading of entanglement in a chaotic system by introducing the

entanglement velocity in this setup. In order to capture the behavior of $S_{\text{vn}}^{\text{reg}}(A \cup B; \alpha)$ around $r_0 \approx r_c$, we first expand $S_{\text{vn}}^{\text{reg}}(A \cup B; \alpha)$ up to linear order in $(r - r_0)$. This leads to the following form:

$$\begin{aligned} S_{\text{vn}}^{\text{reg}}(A \cup B; \alpha) &\approx 2L^{d-2} \sqrt{-f(r_0)} r_0^{p(d-1)} \int_{r_0}^{r_+} \frac{dr}{r_0^{2p} f(r_0) \sqrt{\left(-\frac{2p(d-1)}{r_0} - \frac{f'(r_0)}{f(r_0)}\right)(r - r_0)}} \\ &= 2L^{d-2} \sqrt{-f(r_0)} r_0^{p(d-1)} \int_{r_0}^{r_+} \frac{dr}{r_0^{2p} f(r_0)} \left[1 - \frac{1}{\sqrt{\left(-\frac{2p(d-1)}{r_0} - \frac{f'(r_0)}{f(r_0)}\right)(r - r_0)}} \right] \\ &\quad - 2L^{d-2} \sqrt{-f(r_0)} r_0^{p(d-1)} \int_{r_0}^{r_+} \frac{dr}{r_0^{2p} f(r_0)}. \end{aligned} \quad (79)$$

Now, by using the relation given in Eq. (75), we can write down the following form of $S_{\text{vn}}^{\text{reg}}(A \cup B; \alpha)$ and proceed to consider the $r_0 \rightarrow r_c$ limit,

$$\begin{aligned} S_{\text{vn}}^{\text{reg}}(A \cup B; \alpha) &\approx 2L^{d-2} \sqrt{-f(r_0)} r_0^{p(d-1)} \\ &\quad \times \left(\frac{\beta}{4\pi} \log \alpha(r_0) \right) \Big|_{r_0=r_c}. \end{aligned} \quad (80)$$

Keeping in mind the exponential growth of the given perturbation, that is, $\alpha \sim \exp^{\frac{2\pi}{\beta}t}$, one can write down the following equation [36,38,41–43]:

$$\begin{aligned} \frac{dS_{\text{vn}}^{\text{reg}}(A \cup B; \alpha)}{dt} &= 2L^{d-2} \sqrt{-f(r_c)} r_c^{p(d-1)} \left(\frac{\beta}{4\pi} \right) \left(\frac{2\pi}{\beta} \right) \\ &= 4L^{d-2} \sqrt{-f(r_c)} \left(\frac{r_c}{r_+} \right)^{p(d-1)} \left(\frac{r_+^{p(d-1)}}{4} \right) \\ &= s_{\text{th}} \mathcal{A}_{\Sigma} v_{\text{en}}, \end{aligned} \quad (81)$$

where s_{th} is the thermal entropy density $s_{\text{th}} = \frac{r_+^{p(d-1)}}{4}$, $\mathcal{A}_{\Sigma} = 4L^{d-2}$ is the area of the hyperplane, and v_{en} is the entanglement velocity which has the following form:

$$v_{\text{en}} = \left(\frac{r_c}{r_+} \right)^{p(d-1)} \sqrt{-f(r_c)}. \quad (82)$$

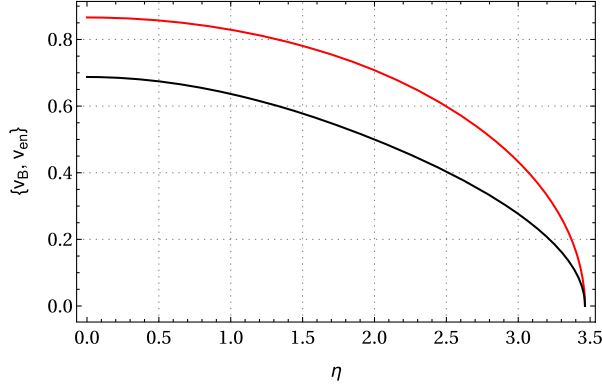


FIG. 10. Comparison between the variations of the butterfly velocity (the upper curve) and entanglement velocity (the lower curve) with respect to the nonconformal parameter η .

By using the explicit value of r_c [given in Eq. (76)], one can obtain an exact expression for the entanglement velocity. This reads as

$$v_{en} = \left[1 - \frac{c}{2p(d-1)} \right]^{\frac{p(d-1)}{c}} \sqrt{\frac{c}{2p(d-1) - c}}. \quad (83)$$

In the limit $\eta \rightarrow 0$, one obtains the standard conformal result (result for SAdS_{d+1}). This reads as [36]

$$v_{en} = \frac{\sqrt{d(d-2)}^{\frac{1}{2}-\frac{1}{d}}}{[2(d-1)]^{1-\frac{1}{d}}}. \quad (84)$$

From our obtained result of entanglement velocity [given in Eq. (83)], we observe that similar to the butterfly velocity and Lyapunov exponent, it also decreases with the increase in the value of the nonconformal parameter η . Furthermore, v_{en} also vanishes for $\eta = \sqrt{\frac{8d}{d-1}}$ representing the complete disruption of quantum entanglement. We have represented our observations graphically in Fig. 10. Figure 10 also reveals that in the presence of nonconformality, entanglement velocity still satisfies the property $v_{en} \leq v_B$. Further, both of these velocities are always less than the speed of light (as speed of light $v_c = 1$).

V. POLE-SKIPPING ANALYSIS: LYAPUNOV EXPONENT AND BUTTERFLY VELOCITY

In this section, we will point out the special points, known as the pole-skipping points, in the complex (ω, k) plane at which the near-horizon solution of the bulk field is ill defined which leads to the nonunique nature of the corresponding retarded Green's function. As mentioned earlier, the location of these points in the complex (ω, k) (upper half or lower half) depends on the spin s of the bulk field. As we have already shown in Eq. (10), only the upper half pole-skipping points are related to the Lyapunov exponent and the butterfly velocity. As we are interested

in the near-horizon analysis of the bulk field equation of motion, we recast the bulk metric [given in Eq. (13)] in the ingoing Eddington-Finkelstein coordinate system,

$$v = t + r_*. \quad (85)$$

In the above coordinate system, the bulk metric takes the following form:

$$ds^2 = -r^{2p} f(r) dv^2 + 2dvdr + h(r) \sum_{i=1}^{d-1} dx_i^2, \quad h(r) = r^{2p}. \quad (86)$$

On the other hand, we assume the following linear perturbation of the metric and the dilaton field (in the x_1 direction):

$$\begin{aligned} \delta g_{\mu\nu}(v, r, x_1) &= \delta g_{\mu\nu}(r) e^{-i\omega v + ikx_1} \\ \delta\phi(v, r, x_1) &= \delta\phi(r) e^{-i\omega v + ikx_1}. \end{aligned} \quad (87)$$

In the sound mode, the relevant perturbations are δg_{vv} , δg_{vr} , δg_{vx_1} , δg_{rr} , δg_{rx_1} , $\delta g_{x_i x_i}$ along with $\delta\phi$ which can couple to any of these metric fluctuations. As the location of the pole-skipping point (ω_*, k_*) depends on the behavior of the background metric on the horizon, one has to consider the near-horizon behavior of these perturbations [45,46,69]. In the near-horizon regime, the perturbations behave in the following way:

$$\begin{aligned} \delta g_{\mu\nu}(r) &= \delta g_{\mu\nu}^{(0)} + \delta g_{\mu\nu}^{(1)}(r - r_+) + \mathcal{O}(r - r_+)^2 \dots \\ \delta\phi(r) &= \delta\phi^{(0)} + \delta\phi^{(1)}(r - r_+) + \mathcal{O}(r - r_+)^2 \dots \end{aligned} \quad (88)$$

We now follow the approach given in [45].

By substituting the above forms of perturbations in the Einstein field equations [given in Eq. (12)] and by considering the near-horizon limit, one observes that the vv component of the Einstein-field equation assumes the following universal form [45]:

$$\begin{aligned} &\left(-i \frac{(d-1)}{2} \omega h'(r_+) + k^2 \right) \delta g_{vv}^{(0)} \\ &- i(2\pi T_H + i\omega) \left(\omega \delta g_{x_i x_i}^{(0)} + 2k \delta g_{vx_1}^{(0)} \right) = 0. \end{aligned} \quad (89)$$

By incorporating the background metric information from Eq. (86), we obtain the following form for the case we have in hand:

$$\begin{aligned} &\left(-i \frac{(d-1)}{2} \omega \partial_r r^{2p} |_{r=r_+} + k^2 \right) \delta g_{vv}^{(0)} \\ &- i(2\pi T_H + i\omega) \left(\omega \delta g_{x_i x_i}^{(0)} + 2k \delta g_{vx_1}^{(0)} \right) = 0. \end{aligned} \quad (90)$$

From the above equation, one can easily point out the special values of ω and k for which the equation gets satisfied. The values of ω read as

$$\omega = i2\pi T_H \equiv \omega_*. \quad (91)$$

On the other hand, for k , the corresponding special value is given by

$$k = \sqrt{i \frac{(d-1)}{2} \omega_* \partial_r r^{2p} |_{r=r_+}} = i \frac{2\pi T_H}{\sqrt{\frac{c}{2p(d-1)}}} = k_*. \quad (92)$$

We now make use of the relations given in Eq. (10) along with the above obtained values of ω_* and k_* to obtain the following results:

$$\lambda_L = \frac{2\pi}{\beta} \quad (93)$$

$$v_B = \sqrt{\frac{c}{2p(d-1)}} \equiv \frac{1}{4} \sqrt{\frac{8d}{d-1} - \eta^2}. \quad (94)$$

The above results agrees perfectly with that obtained from the shock wave analysis [Eq. (53)]. A few remarks are in order now. From the above computation, one can conclude that the metric perturbation in the sound channel leads to the energy density Green's functions which have the pole-skipping points in the upper half of the complex (ω, k) plane. The importance of these points lying in the upper half plane is that they lead to the parameters of chaos, based upon the relations given in Eq. (10). This further verifies the previously mentioned statement that for a strongly coupled theory with holographic dual which is maximally chaotic, the pole-skipping points are related to the parameters of chaos. However, it is to be kept in mind that the association of the pole-skipping points with the parameters of chaos can be made as long as the pole-skipping points are in the upper half of the complex (ω, k) plane. In the Appendix, we show that for a scalar field perturbation, the pole-skipping points lie in the lower half of the complex (ω, k) plane and hence are not related to the parameters of chaos even for a maximally chaotic system.

VI. CONCLUSION

We now summarize our findings. In this work, we have holographically studied the behavior of the parameters of chaos in the presence of nonconformality. By incorporating the gauge/gravity framework, we have introduced the two-sided black hole geometry which is the well-known dual description for the thermofield double state. This realization helps us to quantify the effects of chaos on the correlation which exists between the right and left boundary theories of the two-sided geometry. The

nonconformality in the boundary theories has been holographically introduced by considering the black brane solution of the Einstein-dilaton theory where the dilaton potential is of Liouville type. The asymptote of the black brane geometry is a warped geometry instead of a pure AdS geometry. This implies that the boundary theory is nonconformal as the scale transformations are broken; however, it is relativistic as the Poincaré symmetry is still restored. The black brane solution is associated with a parameter η which characterizes the deviation from conformality as in the limit $\eta \rightarrow 0$, one obtains the usual Schwarzschild black brane solution. In order to keep things general, we have considered the gravitational theory is $(d+1)$ -dimensional which in turn means the boundary theories are d -dimensional. In order to compute the parameters of chaos which are the Lyapunov exponent and the butterfly velocity, we obtain the shock wave geometry corresponding to the black brane solution under consideration. The shock wave geometry arises due to the introduction of a tiny pulse of energy in the geometry (or in dual sense, adding of perturbation at the boundary theory). Owing to the presence of the event horizon, the energy of the pulse gets blueshifted resulting in a nontrivial modification to the original geometry. The obtained results for the Lyapunov exponent and butterfly velocity from the shock wave analysis reveal some interesting observations. We observed that the form of the Lyapunov exponent remains unchanged, that is, $\lambda_L = 2\pi T_H$, as this form is universal for any maximally chaotic holographic theory. It is important to note that the Lyapunov exponent depends only on the Hawking temperature T_H (which is also the temperature of the dual field theory). On the other hand, the effect of nonconformality on the butterfly velocity (v_B) is pretty straightforward to see from the computed expression. Further, we observe that v_B decreases with an increase in the value of the nonconformal parameter η , and finally it vanishes for $\eta = \sqrt{\frac{8d}{d-1}}$. We believe this represents Lyapunov stability for the system as for this particular value of η , the Hawking temperature of the black brane becomes zero (irrespective of the value of r_+) which leads to the vanishing of the Lyapunov exponent, that is, $\lambda_L = 0$. This particular value of η matches perfectly with the previously known upper bound of η , known as the Gubser bound. Our results also confirm the value of this bound from the point of view of chaos. Our results also indicate that nonconformality helps to suppress the chaotic nature for a system. On the other hand, it is a well-known fact that the left and right boundary theories of a two-sided geometry share a nonvanishing quantum correlation between them which can be characterized by the thermomutual information between the mentioned two sides. In order to observe the effects of chaos and nonconformality, we compute the HTMI both in the presence and absence of the shock wave. We observe that nonconformality increases

the existing entanglement between the boundary theories, namely, A and B . This can be understood from the behavior of $S_{\text{vn}}^{\text{reg}}(A \cup B; \alpha)$ as its value increases with the increase in the value of η (for a fixed value of the shock wave parameter $\log \alpha$). We also note that there is a critical value for r_0 , namely, r_c at which the shock wave parameter diverges. Furthermore, an increase in the value of η decreases the value of r_c . This in turn means that the presence of nonconformality helps us to probe further the black hole interior as the point r_0 resides inside the black hole interior. In order to understand the spreading of entanglement for a chaotic system, we proceed to compute the entanglement velocity. We observe that similar to the butterfly velocity, this quantity also decreases with the increase in nonconformality, maintaining the bound $v_B < v_{en}$. Finally, we once again obtain the Lyapunov exponent and butterfly velocity from the lowest pole-skipping points in the upper half of the complex- (ω, k) plane. We observe that the obtained results match perfectly with that obtained from the shock wave analysis. We also compute higher order pole-skipping points [in the lower half of the complex- (ω, k) plane] by considering scalar field fluctuation in the bulk geometry and give the results in the Appendix.

$$p(d-1)r^{p(d-1)-1}\partial_v\Psi + 2r^{p(d-1)}\partial_v\partial_r\Psi + p(d+1)r^{p(d+1)-1}f(r)\partial_r\Psi + r^{p(d+1)}f'(r)\partial_r\Psi + r^{p(d+1)}f(r)\partial_r^2\Psi + r^{p(d-3)}\partial_{x_1}^2\Psi - r^{p(d-1)}m^2\Psi = 0. \quad (\text{A2})$$

We now consider the following Fourier decomposition of the massive scalar field:

$$\Psi(v, r, x_1) = \psi(r)e^{-i\omega v + ikx_1}. \quad (\text{A3})$$

By substituting Eq. (A3) in Eq. (A2), we obtain

$$\psi''(r) + \Delta_1(r)\psi'(r) + \Delta_2(r)\psi(r) = 0, \quad (\text{A4})$$

where

$$\Delta_1(r) = \frac{r^{2p}f'(r) + p(d+1)r^{2p-1}f(r) - 2i\omega}{r^{2p}f(r)}$$

$$\Delta_2(r) = -\frac{\frac{k^2}{r^{2p}} + m^2 + \frac{i\omega}{r}p(d-1)}{r^{2p}f(r)}. \quad (\text{A5})$$

In order to find out the pole-skipping points, one needs to consider the near-horizon limit. The near-horizon expansion for the scalar field reads $\psi(r)$ as

$$\psi(r) = \psi_0 + \psi_1(r - r_+) + \psi_2(r - r_+)^2 + \dots \quad (\text{A6})$$

By substituting the above near-horizon form of $\psi(r)$ in Eq. (A4) and by equating the coefficients of $(r - r_+)^j$ (for $j = 0, 1, 2, \dots$) to zero, one obtains a set of linear equations which read as

ACKNOWLEDGMENTS

A. S. would like to thank S. N. Bose National Centre for Basic Sciences for the financial support through its Advanced Postdoctoral Research Programme. The authors would like to thank the referees for valuable comments and suggestions.

APPENDIX: SCALAR FIELD PERTURBATION AND POLE-SKIPPING POINTS IN THE LOWER HALF OF THE COMPLEX (ω, k) PLANE

In this appendix, we compute the pole-skipping points by considering scalar field fluctuations in the gravitational background. We start our analysis by considering a minimally coupled massive scalar field $\Psi(v, r, x_1)$, the equation of motion for which is governed by the following Klein-Gordon equation:

$$\frac{1}{\sqrt{-g}}\partial_\mu(\sqrt{-g}g^{\mu\nu}\partial_\nu\Psi) - m^2\Psi = 0, \quad (\text{A1})$$

with the background metric being given by Eq. (86).

The above equation assumes the following form in the Eddington-Finkelstein coordinate:

$$\begin{aligned} \chi_{00}\psi_0 + \chi_{01}\psi_1 &= 0, \\ \chi_{10}\psi_0 + \chi_{11}\psi_1 + \chi_{12}\psi_2 &= 0, \\ \chi_{20}\psi_0 + \chi_{21}\psi_1 + \chi_{22}\psi_2 + \chi_{23}\psi_3 &= 0 \\ &\dots, \end{aligned} \quad (\text{A7})$$

where

$$\begin{aligned} \chi_{00} &= -\left(\frac{k^2}{r_+^{2p}} + m^2 + \frac{i\omega}{r_+}p(d-1)\right) \\ \chi_{01} &= r_+^{2p}f'(r_+) - 2i\omega \\ \chi_{10} &= 0 \\ \chi_{11} &= 2r_+^{2p}f''(r_+) + p(d+1)r_+^{2p-1}f'(r_+) \\ &\quad - \left(\frac{k^2}{r_+^{2p}} + m^2 + \frac{i\omega}{r_+}p(d-1)\right) \\ \chi_{12} &= 4r_+^{2p}f'(r_+) - 4i\omega \\ &\dots \\ &\dots \\ &\dots \end{aligned} \quad (\text{A8})$$

The coefficients χ_{ij} can be arranged to form a square matrix:

$$\mathcal{M} = \begin{bmatrix} \chi_{00} & \chi_{01} & 0 & 0 & \dots \\ \chi_{10} & \chi_{11} & \chi_{12} & 0 & \dots \\ \chi_{20} & \chi_{21} & \chi_{22} & \chi_{23} & \dots \\ \dots & \dots & \dots & \dots & \dots \end{bmatrix}.$$

The pole-skipping points are to be obtained by simultaneously solving the equations [46]

$$\chi_{n-1n} = 0; \quad \det(\mathcal{M}) = 0. \tag{A9}$$

We now provide the locations of some of these pole-skipping points. These read as

$$\begin{aligned} \omega_1 = -i2\pi T_H; \quad k_1 &= -i \frac{2\pi T_H}{\sqrt{\frac{c}{2p(d-1)}}} \left[1 + \frac{m^2}{2p(d-1)\pi} \left(\frac{4\pi}{c} \right)^{\frac{1}{(2p-1)}} T_H^{\frac{2-2p}{2p-1}} \right]^{1/2}, \\ \omega_2 = -i4\pi T_H; \quad k_2 &= -i \frac{4\pi T_H}{\sqrt{\frac{c}{p(d-1)+2(c+1)-p(d+1)}}} \left[1 + \frac{m^2}{(4\pi)^2} \left(\frac{c}{p(d-1)+2(c+1)-p(d+1)} \right) \left(\frac{4\pi}{c} \right)^{\frac{2p}{2p-1}} T_H^{\frac{2-2p}{2p-1}} \right]^{1/2}, \\ &\dots \\ &\dots \\ &\dots \end{aligned}$$

From the above one can observe that the pole-skipping points reside in the lower half of the complex (ω, k) plane. This is quite expected from the relation given in Eq. (9) as we have considered scalar field fluctuation which has spin $s = 0$. These points are not related to the parameters of chaos as they are negative.

[1] H.-J. Stöckmann, *Quantum Chaos: An Introduction* (Cambridge University Press, Cambridge, England, 1999).
 [2] D. Ullmo and S. Tomsovic, Introduction to quantum chaos, <http://www.lptms.u-psud.fr/membres/ullmo/Articles/eolss-ullmo-tomsovic.pdf> (2014).
 [3] A. I. Larkin and Y. N. Ovchinnikov, Quasiclassical method in the theory of superconductivity, *J. Exp. Theor. Phys.*
 [4] S. H. Shenker and D. Stanford, Black holes and the butterfly effect, *J. High Energy Phys.* **03** (2014) 067.
 [5] D. A. Roberts and B. Swingle, Lieb-Robinson bound and the butterfly effect in quantum field theories, *Phys. Rev. Lett.* **117**, 091602 (2016).
 [6] E. H. Lieb and D. W. Robinson, The finite group velocity of quantum spin systems, *Commun. Math. Phys.* **28**, 251 (1972).
 [7] S. H. Shenker and D. Stanford, Stringy effects in scrambling, *J. High Energy Phys.* **05** (2015) 132.
 [8] D. A. Roberts, D. Stanford, and L. Susskind, Localized shocks, *J. High Energy Phys.* **03** (2015) 051.
 [9] D. Stanford, Many-body chaos at weak coupling, *J. High Energy Phys.* **10** (2016) 009.
 [10] J. Maldacena, S. H. Shenker, and D. Stanford, A bound on chaos, *J. High Energy Phys.* **08** (2016) 106.
 [11] V. Jahnke, Recent developments in the holographic description of quantum chaos, *Adv. High Energy Phys.* **2019**, 9632708 (2019).
 [12] Y. Sekino and L. Susskind, Fast scramblers, *J. High Energy Phys.* **10** (2008) 065.
 [13] N. Lashkari, D. Stanford, M. Hastings, T. Osborne, and P. Hayden, Towards the fast scrambling conjecture, *J. High Energy Phys.* **04** (2013) 022.
 [14] J. M. Maldacena, The large N limit of superconformal field theories and supergravity, *Adv. Theor. Math. Phys.* **2**, 231 (1998).
 [15] S. S. Gubser, I. R. Klebanov, and A. M. Polyakov, Gauge theory correlators from noncritical string theory, *Phys. Lett. B* **428**, 105 (1998).
 [16] E. Witten, Anti-de Sitter space and holography, *Adv. Theor. Math. Phys.* **2**, 253 (1998).
 [17] S. Grozdanov, On the connection between hydrodynamics and quantum chaos in holographic theories with stringy corrections, *J. High Energy Phys.* **01** (2019) 048.

- [18] M. Natsuume and T. Okamura, Pole-skipping with finite-coupling corrections, *Phys. Rev. D* **100**, 107 (2019).
- [19] W. Israel, Thermo field dynamics of black holes, *Phys. Lett.* **57A**, 107 (1976).
- [20] J. M. Maldacena, Eternal black holes in anti-de Sitter, *J. High Energy Phys.* **04** (2003) 021.
- [21] I. A. Morrison and M. M. Roberts, Mutual information between thermo-field doubles and disconnected holographic boundaries, *J. High Energy Phys.* **07** (2013) 081.
- [22] M. M. Wolf, F. Verstraete, M. B. Hastings, and J. I. Cirac, Area laws in quantum systems: Mutual information and correlations, *Phys. Rev. Lett.* **100**, 070502 (2008).
- [23] P. Hayden, M. Headrick, and A. Maloney, Holographic mutual information is monogamous, *Phys. Rev. D* **87**, 046003 (2013).
- [24] W. Fischler, A. Kundu, and S. Kundu, Holographic mutual information at finite temperature, *Phys. Rev. D* **87**, 126012 (2013).
- [25] T. Dray and G. 't Hooft, The gravitational shock wave of a massless particle, *Nucl. Phys.* **B253**, 173 (1985).
- [26] K. Sfetsos, On gravitational shock waves in curved spacetimes, *Nucl. Phys.* **B436**, 721 (1995).
- [27] S. Leichenauer, Disrupting entanglement of black holes, *Phys. Rev. D* **90**, 046009 (2014).
- [28] N. Sircar, J. Sonnenschein, and W. Tangarife, Extending the scope of holographic mutual information and chaotic behavior, *J. High Energy Phys.* **05** (2016) 091.
- [29] V. Jahnke, Delocalizing entanglement of anisotropic black branes, *J. High Energy Phys.* **01** (2018) 102.
- [30] W.-H. Huang, Butterfly velocity in quadratic gravity, *Classical Quantum Gravity* **35**, 195004 (2018).
- [31] D. Ávila, V. Jahnke, and L. Patiño, Chaos, diffusivity, and spreading of entanglement in magnetic branes, and the strengthening of the internal interaction, *J. High Energy Phys.* **09** (2018) 131.
- [32] W. Fischler, V. Jahnke, and J. F. Pedraza, Chaos and entanglement spreading in a non-commutative gauge theory, *J. High Energy Phys.* **11** (2018) 072; **02** (2021) 149(E).
- [33] D. S. Ageev, Butterflies dragging the jets: On the chaotic nature of holographic QCD, *Phys. Rev. D* **104**, 126013 (2021).
- [34] S. Mahish and K. Sil, Quantum information scrambling and quantum chaos in little string theory, *J. High Energy Phys.* **08** (2022) 041.
- [35] S. Chakraborty, H. Hoshino, S. Pant, and K. Sil, A holographic study of the characteristics of chaos and correlation in the presence of backreaction, *Phys. Lett. B* **838**, 137749 (2023).
- [36] T. Hartman and J. Maldacena, Time evolution of entanglement entropy from black hole interiors, *J. High Energy Phys.* **05** (2013) 014.
- [37] T. Hartman and N. Afkhami-Jeddi, Speed limits for entanglement, [arXiv:1512.02695](https://arxiv.org/abs/1512.02695).
- [38] M. Mezei, On entanglement spreading from holography, *J. High Energy Phys.* **05** (2017) 064.
- [39] P. Calabrese and J. L. Cardy, Evolution of entanglement entropy in one-dimensional systems, *J. Stat. Mech.* (2005) P04010.
- [40] J. S. Cotler, M. P. Hertzberg, M. Mezei, and M. T. Mueller, Entanglement growth after a global quench in free scalar field theory, *J. High Energy Phys.* **11** (2016) 166.
- [41] H. Liu and S. J. Suh, Entanglement tsunami: Universal scaling in holographic thermalization, *Phys. Rev. Lett.* **112**, 011601 (2014).
- [42] H. Liu and S. J. Suh, Entanglement growth during thermalization in holographic systems, *Phys. Rev. D* **89**, 066012 (2014).
- [43] M. Mezei and D. Stanford, On entanglement spreading in chaotic systems, *J. High Energy Phys.* **05** (2017) 065.
- [44] X.-L. Qi and Z. Yang, Butterfly velocity and bulk causal structure, [arXiv:1705.01728](https://arxiv.org/abs/1705.01728).
- [45] M. Blake, R. A. Davison, S. Grozdanov, and H. Liu, Many-body chaos and energy dynamics in holography, *J. High Energy Phys.* **10** (2018) 035.
- [46] M. Blake, R. A. Davison, and D. Vegh, Horizon constraints on holographic Green's functions, *J. High Energy Phys.* **01** (2020) 077.
- [47] M. Natsuume, *AdS/CFT Duality User Guide* (Springer, Tokyo 2015).
- [48] H. Năstase, *Introduction to the AdS/CFT Correspondence* (Cambridge University Press, Cambridge, England, 2015).
- [49] S. Grozdanov, K. Schalm, and V. Scopelliti, Black hole scrambling from hydrodynamics, *Phys. Rev. Lett.* **120**, 231601 (2018).
- [50] S. Grozdanov, P. K. Kovtun, A. O. Starinets, and P. Tadić, The complex life of hydrodynamic modes, *J. High Energy Phys.* **11** (2019) 097.
- [51] M. Natsuume and T. Okamura, Holographic chaos, pole-skipping, and regularity, *Prog. Theor. Exp. Phys.* **2020**, 013B07 (2020).
- [52] M. Natsuume and T. Okamura, Nonuniqueness of Green's functions at special points, *J. High Energy Phys.* **12** (2019) 139.
- [53] N. Ceplak, K. Ramdial, and D. Vegh, Fermionic pole-skipping in holography, *J. High Energy Phys.* **07** (2020) 203.
- [54] N. Ceplak and D. Vegh, Pole-skipping and Rarita-Schwinger fields, *Phys. Rev. D* **103**, 106009 (2021).
- [55] D. Wang and Z.-Y. Wang, Pole skipping in holographic theories with bosonic fields, *Phys. Rev. Lett.* **129**, 231603 (2022).
- [56] S. Ning, D. Wang, and Z.-Y. Wang, Pole skipping in holographic theories with gauge and fermionic fields, *J. High Energy Phys.* **12** (2023) 084.
- [57] M. Blake, H. Lee, and H. Liu, A quantum hydrodynamical description for scrambling and many-body chaos, *J. High Energy Phys.* **10** (2018) 127.
- [58] C. Choi, M. Mezei, and G. Sárosi, Pole skipping away from maximal chaos, *J. High Energy Phys.* **02** (2021) 207.
- [59] N. Abbasi and J. Tabatabaei, Quantum chaos, pole-skipping and hydrodynamics in a holographic system with chiral anomaly, *J. High Energy Phys.* **03** (2020) 050.
- [60] Y. Ahn, V. Jahnke, H.-S. Jeong, K.-Y. Kim, K.-S. Lee, and M. Nishida, Pole-skipping of scalar and vector fields in hyperbolic space: Conformal blocks and holography, *J. High Energy Phys.* **09** (2020) 111.

- [61] Y. Ahn, V. Jahnke, H.-S. Jeong, K.-Y. Kim, K.-S. Lee, and M. Nishida, Classifying pole-skipping points, *J. High Energy Phys.* **03** (2021) 175.
- [62] K.-Y. Kim, K.-S. Lee, and M. Nishida, Holographic scalar and vector exchange in OTOCs and pole-skipping phenomena, *J. High Energy Phys.* **04** (2021) 092; **04** (2021) 229(E).
- [63] M. Natsuume and T. Okamura, Pole-skipping and zero temperature, *Phys. Rev. D* **103**, 066017 (2021).
- [64] N. Abbasi and M. Kaminski, Constraints on quasinormal modes and bounds for critical points from pole-skipping, *J. High Energy Phys.* **03** (2021) 265.
- [65] D. M. Ramirez, Chaos and pole skipping in CFT_2 , *J. High Energy Phys.* **12** (2021) 006.
- [66] N. Abbasi and S. Tahery, Complexified quasinormal modes and the pole-skipping in a holographic system at finite chemical potential, *J. High Energy Phys.* **10** (2020) 076.
- [67] K. Sil, Pole skipping and chaos in anisotropic plasma: A holographic study, *J. High Energy Phys.* **03** (2021) 232.
- [68] H. Yuan and X.-H. Ge, Pole-skipping and hydrodynamic analysis in Lifshitz, AdS_2 and Rindler geometries, *J. High Energy Phys.* **06** (2021) 165.
- [69] M. Blake and R. A. Davison, Chaos and pole-skipping in rotating black holes, *J. High Energy Phys.* **01** (2022) 013.
- [70] H. Yuan and X.-H. Ge, Analogue of the pole-skipping phenomenon in acoustic black holes, *Eur. Phys. J. C* **82**, 167 (2022).
- [71] H. Yuan, X.-H. Ge, K.-Y. Kim, C.-W. Ji, and Y. Ahn, Pole-skipping points in 2D gravity and SYK model, *J. High Energy Phys.* **08** (2023) 157.
- [72] G. Yadav, S. S. Kushwah, and A. Misra, Pole-skipping and chaos in too MUCH hot QCD, *J. High Energy Phys.* **05** (2024) 015.
- [73] Y. Ahn, V. Jahnke, H.-S. Jeong, and K.-Y. Kim, Scrambling in hyperbolic black holes: Shock waves and pole-skipping, *J. High Energy Phys.* **10** (2019) 257.
- [74] H.-S. Jeong, K.-Y. Kim, and Y.-W. Sun, Bound of diffusion constants from pole-skipping points: Spontaneous symmetry breaking and magnetic field, *J. High Energy Phys.* **07** (2021) 105.
- [75] H.-S. Jeong, K.-Y. Kim, and Y.-W. Sun, Quasi-normal modes of dyonic black holes and magneto-hydrodynamics, *J. High Energy Phys.* **07** (2022) 065.
- [76] H.-S. Jeong, C.-W. Ji, and K.-Y. Kim, Pole-skipping in rotating BTZ black holes, *J. High Energy Phys.* **08** (2023) 139.
- [77] H.-S. Jeong, Quantum chaos and pole-skipping in a semi-locally critical IR fixed point, [arXiv:2309.13412](https://arxiv.org/abs/2309.13412).
- [78] S. Kulkarni, B.-H. Lee, C. Park, and R. Roychowdhury, Non-conformal hydrodynamics in Einstein-dilaton theory, *J. High Energy Phys.* **09** (2012) 004.
- [79] S. Kulkarni, B.-H. Lee, J.-H. Oh, C. Park, and R. Roychowdhury, Transports in non-conformal holographic fluids, *J. High Energy Phys.* **03** (2013) 149.
- [80] C. Park, Holographic aspects of a relativistic nonconformal theory, *Adv. High Energy Phys.* **2013**, 389541 (2013).
- [81] C. Park, Holographic entanglement entropy in the non-conformal medium, *Phys. Rev. D* **91**, 126003 (2015).
- [82] C. Charmousis, B. Gouteraux, and J. Soda, Einstein-Maxwell-dilaton theories with a Liouville potential, *Phys. Rev. D* **80**, 024028 (2009).
- [83] S. S. Gubser, Curvature singularities: The good, the bad, and the naked, *Adv. Theor. Math. Phys.* **4**, 679 (2000).
- [84] B. Gouteraux and E. Kiritsis, Generalized holographic quantum criticality at finite density, *J. High Energy Phys.* **12** (2011) 036.
- [85] A. Saha, S. Gangopadhyay, and J. P. Saha, Generalized entanglement temperature and entanglement Smarr relation, *Phys. Rev. D* **102**, 086010 (2020).
- [86] X. Y. Chew, D.-h. Yeom, and J. L. Blázquez-Salcedo, Properties of scalar hairy black holes and scalarons with asymmetric potential, *Phys. Rev. D* **108**, 044020 (2023).
- [87] X. Y. Chew and K.-G. Lim, Scalar hairy black holes with inverted Mexican hat potential, *Phys. Rev. D* **109**, 064039 (2024).
- [88] S. H. Shenker and D. Stanford, Multiple shocks, *J. High Energy Phys.* **12** (2014) 046.
- [89] S. Ryu and T. Takayanagi, Holographic derivation of entanglement entropy from AdS/CFT, *Phys. Rev. Lett.* **96**, 181602 (2006).
- [90] S. Ryu and T. Takayanagi, Aspects of holographic entanglement entropy, *J. High Energy Phys.* **08** (2006) 045.
- [91] V. E. Hubeny, M. Rangamani, and T. Takayanagi, A covariant holographic entanglement entropy proposal, *J. High Energy Phys.* **07** (2007) 062.
- [92] A. Kundu, Wormholes and holography: An introduction, *Eur. Phys. J. C* **82**, 447 (2022).
- [93] V. E. Hubeny, Extremal surfaces as bulk probes in AdS/CFT, *J. High Energy Phys.* **07** (2012) 093.